Understanding the Molecular Mechanisms that Drive the Invasive Behaviour of Paediatric Brain Tumours

Major Research Project

Leyla Rigamonti
Drug Innovation, MSc Student (2021-2022)
Student ID: 5450217

Supervisor: Dennis Metselaar, PhD

Examiner: Esther Hulleman, PhD
Second Reviewer: Jens Bunt, PhD

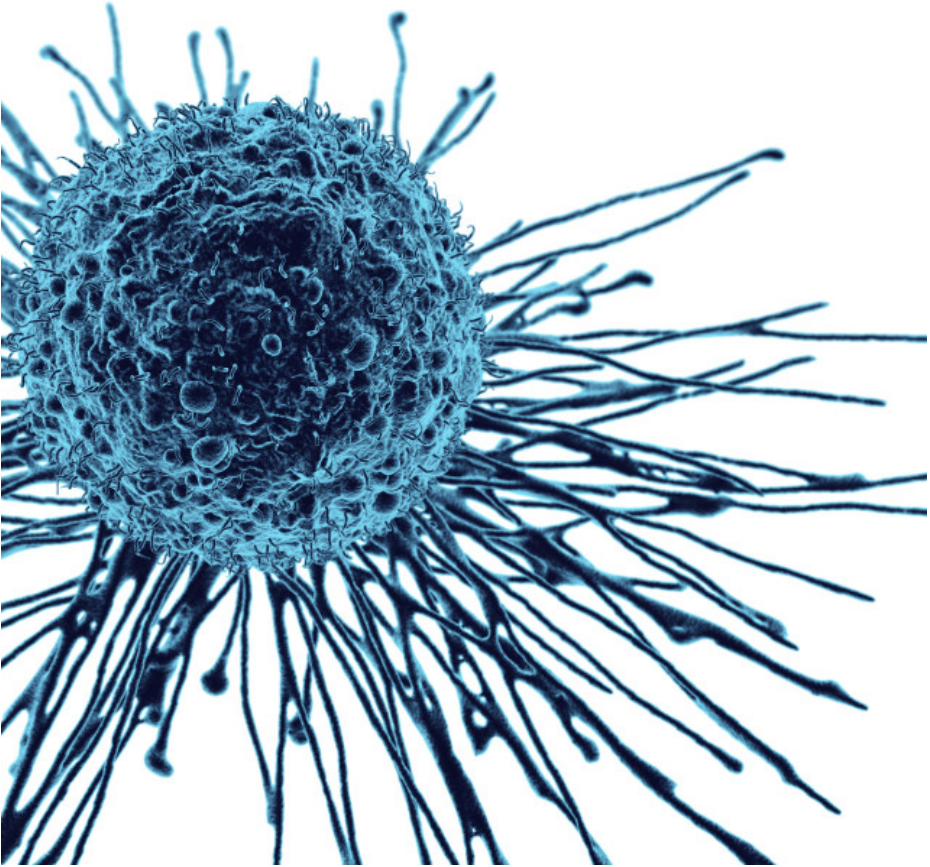

Abstract

Paediatric high-grade gliomas (pHGG) and atypical teratoid rhabdoid tumours (ATRT) are grade IV paediatric central nervous system neoplasms with high morbidity. Due to their diffuse growth patterns, removing or killing all pHGG and ATRT cells is close to impossible, despite advancements in treatment modalities. Therefore, understanding the molecular mechanisms that drive paediatric brain tumour invasion can reveal the genes contributing towards this invasive phenotype, revealing novel therapeutic targets that can inhibit the malignant behaviour. Therefore, this project aimed to optimise a high throughput *in vitro* invasion assay that can be combined with a CRISPR-KO screen to uncover the genetic perturbations that are vital for invasion. To this end, we established several Cas9-expressing pHGG and ATRT cultures and prepared a whole genome CRISPR-KO screen in a VUMC-ATRT-03 cell culture. Furthermore, we tested different invasion assay approaches and concluded that the drop invasion assay described has the greatest potential for high-throughput applications. With this research, we were able to take the first steps necessary for combining a CRISPR-KO screen with an invasion assay to improve our understanding of the biology that drives the invasive behaviour observed in paediatric brain tumours. In the future, this research has the potential of improving treatment outcomes by keeping tumour cells localised to confined regions of the brain and within reach of focused therapies.

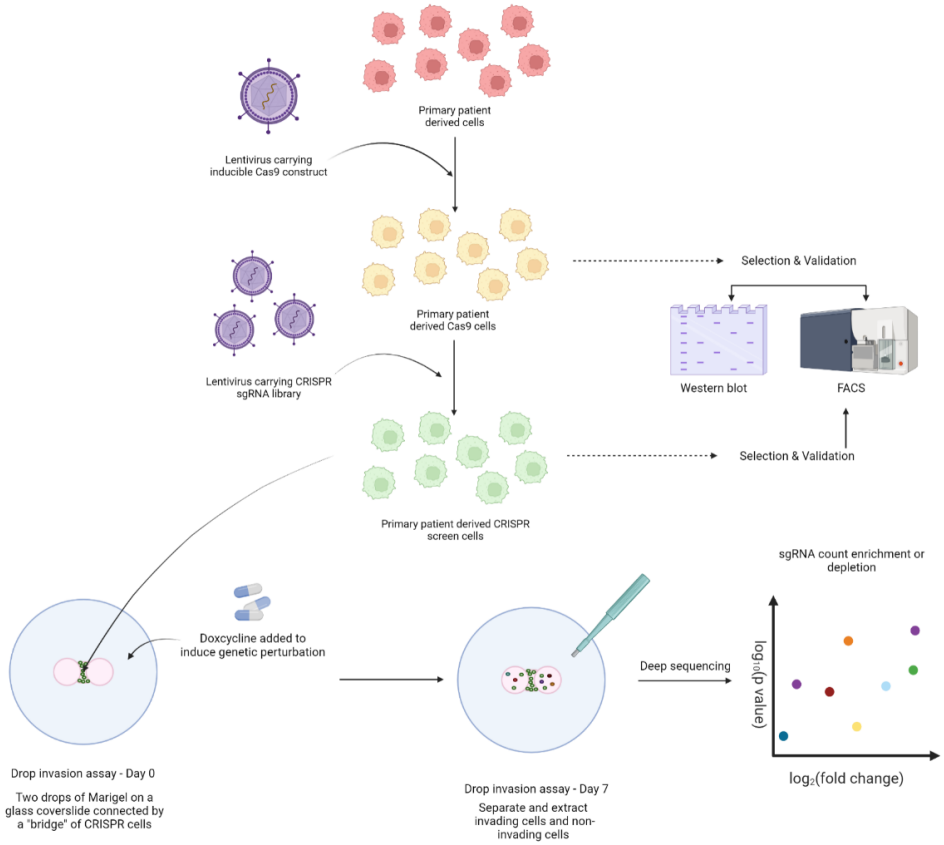

Figure 1: Graphical abstract providing an overview of the project. CRISPR-KO screens can be incorporated into an invasion assay to determine the molecular drivers of pHGG and ATRT invasion *in vitro*. The abstract illustrates the workflow used to prepare cell cultures for CRISPR screening and how the invasion assay is incorporated (made with Biorender.com).

Plain Language Summary

High-grade brain cancers in children are deadly and incurable diseases that affect 10 – 12% of children diagnosed. These cancer types are very invasive, spreading to distant regions of the brain, and make treatments such as surgery and chemotherapy/radiotherapy ineffective for curing the disease as the cancer can be found in all areas of the brain. A good way to improve the effects of surgery and chemotherapy/radiotherapy is to identify ways to stop brain cancers from spreading throughout the brain of children. To achieve this, we aimed to understand what causes brain cancer cells to spread by firstly developing an invasion experiment where we could monitor this cell movement. The invasion experiment simulates the spread of brain cancer cells by using a gel material to mimic the brain. The cancer cells were put inside the gel material and using a microscope we could monitor the cell movements at different timepoints. Finding the best set-up for the experiment is important because we need to be able to distinguish between invading and non-invading cells if we want to understand what allows the cells to spread. Therefore, different set-ups were tested. The second part of this project was focused on preparing the brain cancer cells for the invasion experiment, by altering the DNA of the cancer cells to see if it is possible to stop them from spreading. All the information about a cell is carried in its DNA, which is made up of different genes that can control the function of a cell. To alter the DNA of a cell, we used "Clustered Regularly Interspaced Short Palindromic Repeat" (CRISPR) technology. The CRISPR technology uses an enzyme that can target and switch-off specific genes in the DNA of a cell. By doing so, we can see which genes are important for the spread of brain cancer cells because without the gene, the cells will not be able to spread in the invasion experiment. In this research internship, we concluded that the drop invasion experiment was the best method for monitoring brain cancer invasion because we were able to differentiate between spreading and non-spreading cells. We were also able to successfully prepare the brain cancer cells by using the CRISPR technology to switch-off genes from the DNA. By combining the two parts of this research project, we can identify the genes important for brain cancer cell invasion and use specific drugs to switch-off these genes. Potentially, this information can be used to stop brain cancers from spreading, making it easier for doctors to treat patients and perform surgery.

Table of Contents

Introduction

Paediatric central nervous system (CNS) neoplasms are the most common and lethal solid-tumour type in children.[1,2] Gliomas are primary CNS tumours that arise from glial progenitors, such as astrocytic cells, oligodendrocytes, and ependymal cells, or neuroectodermal stem cells.[3,4] Previously, the categorisation of gliomas was solely based on morphological characteristics.[4,5] However, the continuous advancements in the transcriptomic landscape of paediatric brain tumours have led to the incorporation of molecular parameters in the classification system of CNS tumours.[1,6] Paediatric high-grade gliomas (pHGG) (grade III and IV), such as anaplastic astrocytoma and diffuse midline glioma, represent 10-20% of all paediatric CNS tumours and typically arise from a single somatic variant, making them distinct from adult HGGs.[3,7,8,9] Since 2021, the WHO classification of CNS Tumours has distinguished between 4 paediatric-type diffuse high-grade gliomas: "*Diffuse midline glioma, H3 K27-altered*" (DMG); "*Diffuse hemispheric glioma, H3 G34-mutant"*; "*Diffuse paediatric-type high-grade glioma. H3-wildtype and IDH-wildtype"*; and "*Infant-type hemispheric glioma"*.[6,10] The typical attributes of each of the somatic variants is summarised in **Figure 2**. Overall, the histological hallmarks of pHGGs include nuclear atypia, high mitotic activity, pseudo palisading necrosis, and highly infiltrative growth into surrounding tissue.[3,11,12] This highly invasive phenotype is the characteristic that makes these paediatric-type diffuse high grade gliomas so lethal, allowing individual tumour cells to infiltrate the brain parenchyma and evade treatment. This characteristic coupled with the neoplasms location in vital brain structures, such as the brain stem, make pHGGs much more aggressive than other CNS tumours and expedite tumour progression, thus reflecting the 5-year survival rate of less than 10% in children.[6,13]

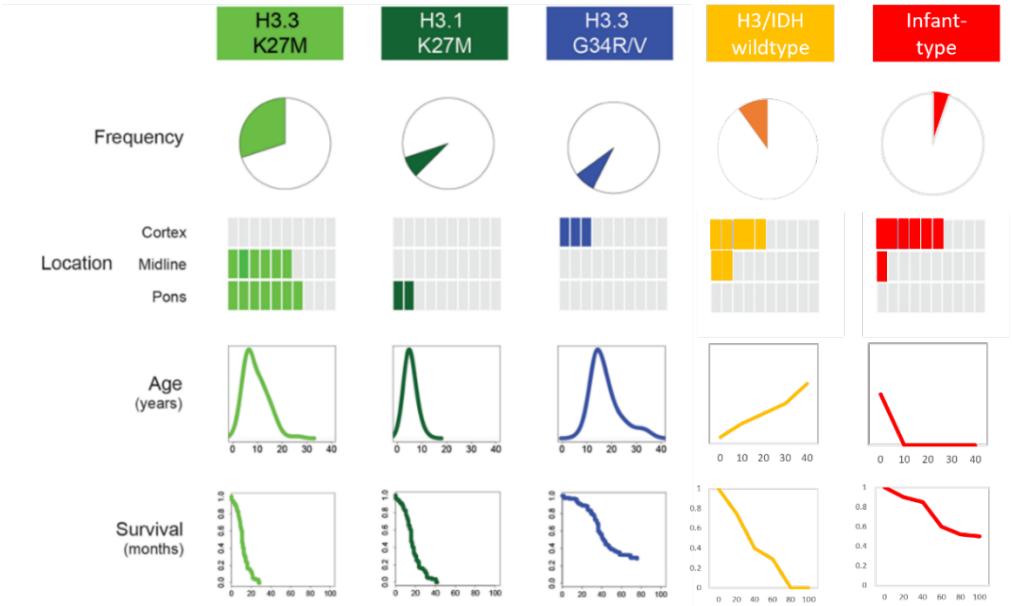

Figure 2: Molecular subtypes of pHGGs based on somatic histone mutations. The figure illustrates the frequency and epidemiology of each subgroup in the paediatric population.[14,15,16]

Another epigenetically dysregulated high-grade paediatric CNS tumour is the atypical teratoid rhabdoid tumour (ATRT). Despite only accounting for 1-2% of all paediatric CNS tumours, ATRTs are relatively common in infants, representing 40-50% of all CNS neoplasms in children under one year of age.[17,18] ATRTs are frequently characterised by the biallelic loss-of-function alterations in *SMARCB1*, a critical subunit of the canonical SWItch/sucrose non-fermentable (SWI-SNF) chromatin remodelling complex (CRC), necessary for cell lineage determination and cell differentiation.[17,19] In less than 5% of cases, loss-of-function alterations in other subunits of the SWI-SNF CRC, such as *SMARCA4* and *ARID1A*, have also been found to be driver genetic lesions of ATRTs.[18,20,21] To date, there are 3 distinct molecular subtypes of ATRTs defined by DNA methylation and gene expression profiling: ATRT with enzyme tyrosinase overexpression (ATRT-TYR), ATRT with overexpression of sonic hedgehog and Notch pathway members (ATRT-SHH) and ATRT with MYC oncogene overexpression (ATRT-MYC).[22] The typical characteristics of each molecular subtype, including location of tumour and age of onset, is summarised in **Figure 3**. Overall, the prognosis of patients diagnosed with ATRT is dire, with less than 50% of patients surviving 1-year post-diagnosis. However, between the different molecular subtypes prognosis has been found to be highly dependent on the age of the patient, localisation of the tumour, and metastatic markers.[17]

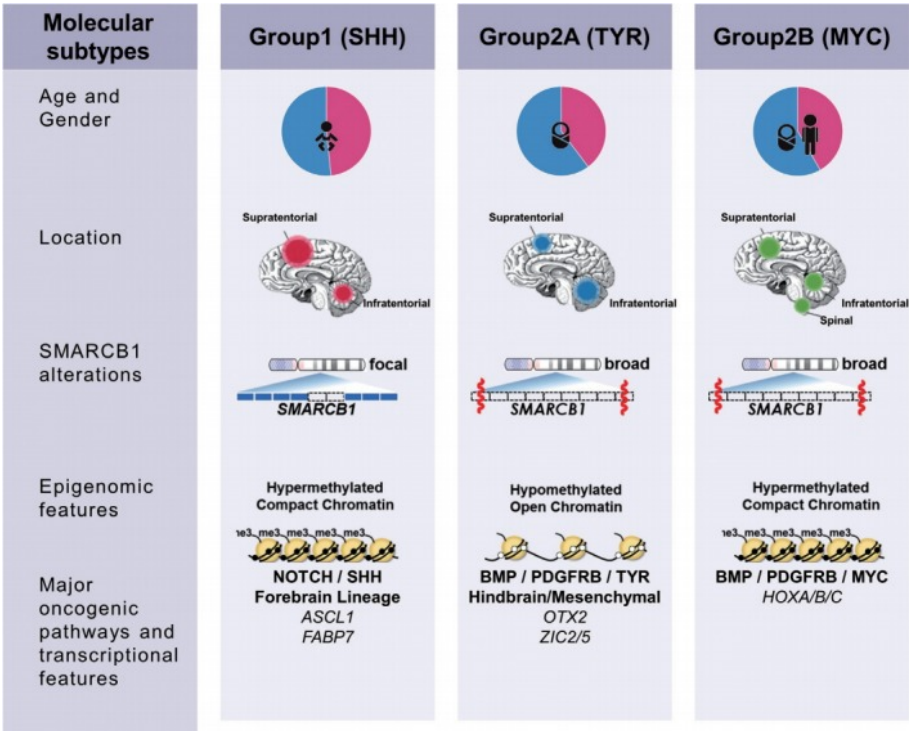

Figure 3: Molecular subtypes of ATRTs. The figure illustrates the localisation, molecular aberrations and epigenomic features that characterise the different ATRT subtypes.[23]

Current Treatments

The molecular subtypes of pHGG and ATRT and their localisation in the CNS largely dictates prognosis of patients. In general, pHGGs of different molecular subtypes are often treated in a similar manner, with a combination of chemotherapy and fractioned radiotherapy.[24,25,26] The only difference in treatment between pHGGs of different molecular backgrounds is the amount

of surgical resection. For DMG patients, the highly diffusive nature and localisation in the pons of the brain stem renders these tumours inoperable.[24] The pons area is the location in which most cranial neurons emerge and vital functions such as respiration and cardiac rhythm are regulated, making it difficult to perform surgery without causing paralysis or fatality.[27] Contrastingly, pHGGs localised in the cerebral hemispheres can often be resected prior to chemotherapy and radiotherapy, perhaps contributing to the more favourable prognosis.[25,28,29] ATRTs are also treated with comparable therapeutic strategies, however, treatments administered to patients varies amongst different institutions and is highly dependent on the patients age.[30] There is hesitancy to use chemotherapy and radiotherapy because both can have serious and irreversible consequences in the development of paediatric patients, such as life-long impact on the development and function of several vital organs, and impaired neurocognitive function, respectively.[12,30,31] Incontestably, patient outcomes remain poor and there is a need to develop increasingly effective therapeutics to target both pHGG and ATRT.[32]

Our improved understanding of the molecular drivers of these devastating paediatric malignancies has led to the discovery of a plethora of potential drug targets preclinically. However, despite convincing laboratory results, this has barely improved pHGG and ATRT prognoses.[33] Often, many of the drugs tested in preclinical phases are not translated to the clinic because of poor drug delivery through the blood-brain-barrier (BBB) (See **in-depth information box** for more details about the BBB). Therefore, recent research has been highly focused on developing novel drug-delivery methods to overcome the BBB. One newly defined technique now being employed for clinical use is convection-enhanced delivery (CED). With CED, cannulas are inserted into the targeted tumour area and are used to deliver the chemotherapeutic agents directly to the tumour.[34] In this way, the BBB is physically overcome, and systemic exposure of the treatment is limited. Another method developed to physically overcome the BBB is with the use of focused ultrasound (FUS). Using FUS pulses, intravenously injected microbubbles in the bloodstream begin to vibrate in response to the sound waves, physically disrupting the BBB by temporarily separating tight junctions in between endothelial cells and increasing BBB permeability.[35,36] This reversible process can be

used to allow small molecules to bypass the BBB in a safe and feasible way and is currently being tested in numerous clinical trials for DMG patients.[36,37]

In-depth Information Box: The Blood-Brain-Barrier

The BBB is a tightly regulated semi-permeable barrier composed of endothelial cells with tight junctions, astrocytic end-feet, pericytes, microglia and neurons, that collectively function to maintain CNS homeostasis.[38,39] The astrocytes in particular play an important role in regulating the exchange of molecules across the BBB by releasing soluble factors that influence specialised transporters located in the tight junctions of endothelial cells.[38] During the development and rapid growth of a brain tumour, the integrity of the BBB often becomes compromised, existing blood vessels are hijacked by tumour cells, and simultaneously new blood vessels are induced through angiogenesis. This can result in the BBB appearing 'leakier' because of the displacement and loss of astrocytic end feet by tumour cells, as well as the uneven distribution of pericytes.[35] Under normal conditions, the BBB only permits the passage of molecules from the bloodstream that are larger than 400 Daltons and lipid soluble.[40] This selective movement of molecules across the BBB means that only 5% of potentially effective therapeutics can reach the area of interest at sufficient concentrations through either paracellular or transcellular pathways.[41]

Despite potentially overcoming the drug delivery limitations associated with the BBB, one recurring issue that is the major driver of tumour relapse is the diffuse growth pattern of pHGGs and ATRTs, often meaning that localised treatments such as CED and FUS fail to target distant areas which have already been infiltrated by the tumour.[42,43] For this reason, it is essential to understand the mechanisms that drive pHGG infiltrative migration as a stepping-stone to inhibit this diffusive growth pattern. The inhibition of tumour invasion would facilitate and improve the effectiveness of precision radiotherapy and chemotherapy by keeping the tumour in a confined area and lowering the possibilities of comorbidities associated with tumour growth in other parts of the CNS.[44] Furthermore, the toxicities associated with targeting a larger area of the brain will also be reduced.

Preclinical Invasion Research

To study the invasive behaviour of cells, researchers have developed several different *in vivo* and *in vitro* assays. Although *in vivo* approaches best represent the tumour microenvironment and the interactions between tumour and non-tumour brain cells, the large costs, time, and complexity, as well as ethical implications, associated with performing such assays makes *in vitro* invasion assays a more appealing approach.[45,46] Invasion assays *in vitro* can be separated into two-dimensional (2D) and three-dimensional (3D) assays. A summary of several *in vitro* invasion assays, together with their respective strengths and limitations is provided in **Table 1**. Ideally, *in vitro* invasion assays should be able to mimic the complexity of the *in vivo* tumour microenvironment, whilst remaining simple enough for researchers to visualise and study the

invasive behaviour of cells. One such way to mimic the tumour microenvironment is through selecting an appropriate bioscaffold, composed of similar components as the extracellular matrix (ECM) of brain tissue. Often 3D invasion assays are performed with ECM materials such as Matrigel, which is enriched in basement membrane proteins such as laminin, entactin and type IV collagen, or type I collagen.[47] However, recent research has highlighted the critical role the CNS ECM plays in tumorigenesis and tumour invasion. One particularly important CNS ECM component is hyaluronan (HA), which also functions as a ligand for the HA-medicated cell motility receptor (RHAMM) and cluster of differentiation 44 (CD44) in GBM.[48] To this end, the HyStem®-HP (HSHP) matrix is theoretically a potential candidate for studying the invasive behaviour of cells *in vitro*. The HSHP is a thiol-modified hyaluronan hydrogel that controllably releases growth factors and is enriched in HA. Unlike Matrigel, the HSHP bioscaffold has not been validated with tumour models and thus it is of pivotal importance to test and compare the functionality of this matrix.

Table 1: A summary of *in vitro* invasion assays. This table briefly describes the different invasion assays and highlights their respective strengths and limitations.

Name	Dimension	Description	Strengths	Limitations
Scratch Assay	2D	A monolayer of cells cultured on a glass or plastic slide.[46]	Simple and extracellular matrix coatings can be used to observe the role extracellular matrix components play in tumour motility.[49]	Motility only.
Transwell Assay	2D	Two chamber system separated by a porous membrane. Cells are seeded into the upper chamber and the ability of cells to invade the lower chamber is assessed.[46]	Simple and parameters such as pore size and chemotactic gradients can be altered.[46,50]	2D cell cultures do not behave the same as 3D cell cultures and method is an oversimplification of *in vivo* situations.[46]
3D Matrigel Invasion	3D	A monolayer of tumour cells is embedded between two layers of Matrigel.[51]	Able to monitor cell invasion and changes in cell morphology.[46]	Matrigel has been reported to have xenogeneic contaminants and variability in composition.[52]
Spheroids	3D	Cells are cultured in suspension to form spheroids and embedded into a 3D extracellular matrix.[46]	Spheroids have oxygen and nutrient gradients like tumours *in vivo*.[52]	Can only be performed on cell types that are able to form spheroids.[52]

CRISPR Knockout Screening

Clustered Regularly Interspaced Short Palindromic Repeat (CRISPR) gene editing is a genome modification tool used in molecular biology to edit genes at specific loci.[54] The CRISPR system is composed of a guide RNA (gRNA) and a CRISPR-associated (Cas9) protein. The Cas9 protein is an endonuclease responsible for creating double strand breaks (DSB) at specific positions of the target DNA.[55] The gRNA is divided into two distinct parts: the trans-activating CRISPR RNA (tracrRNA) that binds the gRNA to the Cas9 nuclease; and the CRISPR RNA (crRNA) that guides the Cas9 nuclease to the target DNA sequence.[55] In this way, the CRISPR/Cas9 system can be used to create blunt-ended DSB at specific loci that will then be repaired by non-homologous end-joining (NHEJ), or homology directed repair (HDR).[54] NHEJ is an error-prone process that occurs in all phases of the cell cycle and in the absence of a repair template, where the DSB is re-ligated, leading to an insertion/deletion (indel) mutation that consequently knockouts (KO) an entire gene.[54,56] Conversely, HDR is only active in dividing cells when a homologous DNA template is present and can be harnessed to execute precise gene insertions.[54,55] Using the CRISPR/Cas9 system, high-throughput screenings can be performed to efficiently identify relevant molecular targets that are responsible for tumour cell invasion, for example. The high-throughput CRISPR knockout (CRISPR-KO) screen entails introducing a pooled gRNA library into Cas9-expressing cells through lentiviral transductions.[57] Each cell will integrate a single gRNA into its genome, where a perturbation can be induced according to the crRNA received by the cell.[57] To reduce undesirable off-target effects caused by constitutively activated Cas9, a doxycycline inducible system can be implemented to transcriptionally control the expression of Cas9 endonuclease.[58] In this way, the exposure of cells to Cas9 and therefore off-target effects is limited. Once the perturbation has been induced through doxycycline exposure, the gene-KO cells are exposed to specific pressures, such as drug treatment, cell proliferation, and cell invasion, so that the fitness of the cells after the genetic perturbation can be determined.[57] Lastly, through deep sequencing the enrichment or depletion of specific gRNAs at different time points, or compared to control conditions, indicates the genes which provide a selective advantage or disadvantage to a specific pressure.[58,59] Therefore, CRISPR-KO screens can theoretically be combined with invasion assays for high-throughput identification of the genes involved in tumour invasion, revealing druggable targets.

Aims

Tumour migration involves a myriad of complex network interactions between the tumour cells, the extracellular matrix, blood vessels, and normal cells of the CNS, amongst others.[60,61] Understanding the molecular mechanisms that drive the invasive growth characteristics of pHGGs and ATRTs can provide insights into the underlying biology behind the invasive behaviour of paediatric brain tumours, subsequently allowing for the identification of novel therapeutic targets that can inhibit the invasive behaviour. The aim of this research project is to optimise an *in vitro* invasion assay that can be combined with CRISPR-KO screens to identify the molecular drivers of pHGG and ATRT invasion in a high-throughput manner. To achieve this, we tested several set-ups for a potential invasion assay that can be used to distinguish invading cells from non-invading cells. This is vital for the second component of the internship, where we aim to successfully establish a CRISPR-KO screen with primary

patient-derived pHGG and ATRT cell cultures. Collectively, these two components of the research project can be combined to identify the genes necessary for the invasive capabilities of ATRT and pHGG cells. Firstly, the CRISPR-KO screen can be used to induce the genetic perturbations in the primary patient-derived cell cultures. The invasion assay will then be used to distinguish and isolate the invading genetically perturbed cells from the non-invading genetically perturbed cells. Finally, through deep sequencing, the distribution of gRNAs between the invading and non-invading cell populations can be determined, revealing the genes that play a pivotal role in ATRT and pHGG invasion. In practice, the findings elucidated in this study can be used to identify druggable targets and test the efficacy of small molecule inhibitors at limiting the diffuse growth patterns of pHGG and ATRT *in vivo*, eventually aiming to rapid clinical translation. Overall, the findings of this research project pave the way for improving the effectiveness of local treatment such as radiotherapy, FUS, and CED, increasing the survival of patients suffering from these devastating malignancies.

Pilot Data

To date, the Hulleman group of the Princess Máxima Center (Utrecht, Netherlands) have established a biobank of primary patient derived cultures, derived from autopsy, biopsy, and resection materials, which are molecularly validated. With these materials, the Hulleman group will provide the tumour models used throughout this project. Furthermore, a well-established protocol has been described by Meel *et al*. (2018) to transduce primary glioma cells using lentiviruses (HSJD-DIPG-07 and VUMC-HGG-11).[62] This was necessary to overcome limitations related to transducing stem cell-like suspension cells such as the primary patient derived pHGGs and ATRTs. Research regarding the conduction of CRISPR screens in primary glioma cells has also been performed, which has provided evidence supporting the feasibility of performing CRISPR screens in primary glioma cells.[63] Additionally, a bioinformatics pipeline is available and can be combined with RNA expression data from the primary patient-derived brain tumour CRISPR-KO screening to identify the differences in behaviour of tumours after specific KOs. Furthermore, U-bottom spheroid invasion assays in Matrigel have already been published in the group, highlighting that the primary patient-derived HSJD-DIPG-07 cells are capable of invading *in vitro*.[64] Therefore, within the Hulleman group, various workflows have been established and will be used for the purpose of this project.

Results

Development of an Invasion Assay Suitable for CRISPR-KO Screenings

To find the optimal approach to monitor the perturbation-induced effects of CRISPR-KO screens on the invading capabilities of pHGG and ATRT, several invasion screen set-ups were designed and subsequently tested using both Matrigel and HSHP. The key characteristics that were deemed optimal for an invasion assay are highlighted in **Table 2**. From these characteristics, several invasion screen methods were designed, which are summarised together with their strengths and weaknesses in **Appendix 2**.

Table 2: Summary of key characteristics that are necessary for the development of an invasion assay that can be combined with high-throughput CRISPR-KO screenings.

Characteristic	Vital characteristics for invasion assay
1	The cells remain viable in the matrix of choice and maintain their capacity to invade
2	Cells can be extracted from the invasion assay to obtain intact sgRNAs
3	In the invasion assay, invading cells can be distinguished from non-invading cells

To test if the HSHP adheres to characteristic 1 as described in **Table 2**, the invasive capabilities of HSJD-DIPG-07, VUMC-DIPG-F and *intra utero* electroporated (IUE)-24B7 (H3.3 K27-altered) murine spheroids in HSHP were determined and compared to Matrigel (**Figure 4**) (**Appendix 1A**). Matrigel was chosen as a comparison because previous research has shown that HSJD-DIPG-07 cells remain viable and invasive in Matrigel.[64] The distance that the spheroids were able to invade at day 0, day 2 and day 6 days was quantified by distinguishing the central neurosphere (red line) from the invasion zone (yellow line) and determining relative invasion (**Figure 4A, 4B**). The imaging results indicated that HSHP is an inappropriate bioscaffold for an invasion assay because the tumour spheroids were unable to invade the gel. Conversely, Matrigel appeared to allow the cells from the spheroids to invade. Therefore, it was concluded that the HSHP does not permit tumour cells to invade through the matrix.

Since the HSHP matrix was unsuitable for tumour cell invasion, it was not necessary to determine if cells could be extracted (characteristic 2 as described in **Table 2**). Furthermore, RNA isolation protocol from Matrigel cultures have already been thoroughly described and is therefore also not investigated in this project.[65]

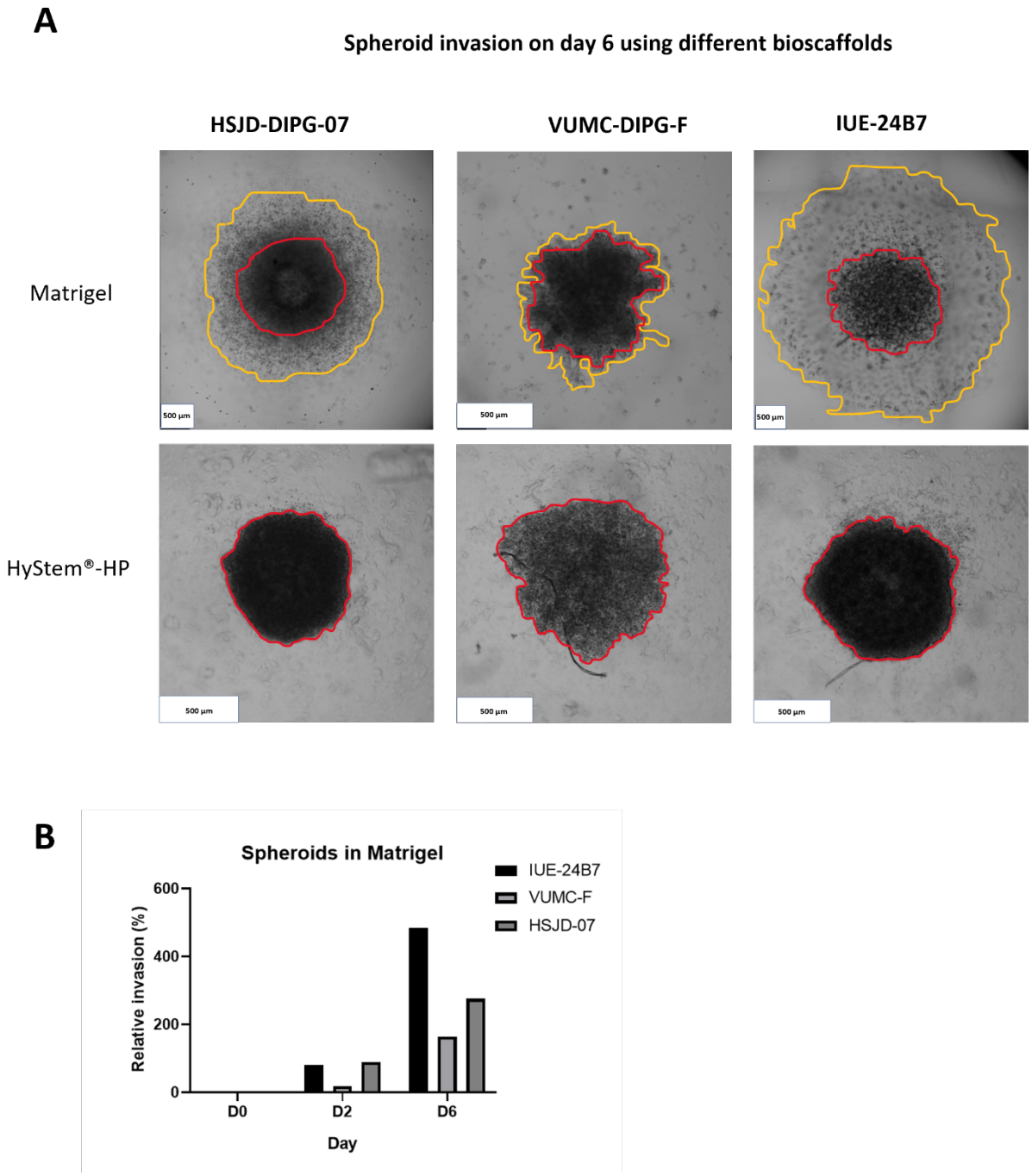

Figure 4: Cells can invade Matrigel. A. Images of HSJD-DIPG-07, VUMC-DIPG-F and IUE-24B7 spheroids after 6 days in Matrigel or HSHP. The red line depicts the core of the spheroid. The yellow depicts the area invaded by tumour cells. **B.** Quantification of relative invasion (%) (n = 1) at day 0, day 2 and day 6.

The final requirement for an invasion assay that can be combined with high-throughput CRISPR-KO screening is that invading cells must be distinguishable from non-invading cells (characteristic 3 as described in **Table 2**). To this end, a system was designed using different layers of matrix and a BacMam 2.0 molecule that would be used to fluorescently tag migrating cells (**Appendix 1B**) (**Figure 5**). The BacMam 2.0 uses a baculovirus as a vehicle to transduce a fusion construct of human tubulin and emGFP into mammalian cells with which it encounters

(**Figure 5A, 5B**). It is important that the molecule used to tag migrating cells is stable and large enough to not to diffuse through the gel and consequently tag non-invading cells. The BacMam 2.0 technology was incorporated into a vertical layer of HSHP matrix, adjacent to a layer of HSHP matrix containing HSJD-DIPG-07 cells (**Figure 5C, 5D**). However, layering of the bioscaffold in a 96-well plate created uneven surfaces, distorting the reproducibility of the method. Furthermore, the BacMam 2.0 technology did not work in this set-up, since only Hoeschst stained invading cells were visible (**Video 1:**https://prinsesmaximacentrum-my.sharepoint.com/:v:/g/personal/l_rigamonti_prinsesmaximacentrum_nl/EcuL2NtzgFhKkcRo7EEfEpIBjy_ceuoPH5Vv00CqNFEedw?e=euvMmP). Therefore, we concluded that the three-layer approach was inappropriate for an invasion assay, as it did not meet criteria 3 of **Table 2**.

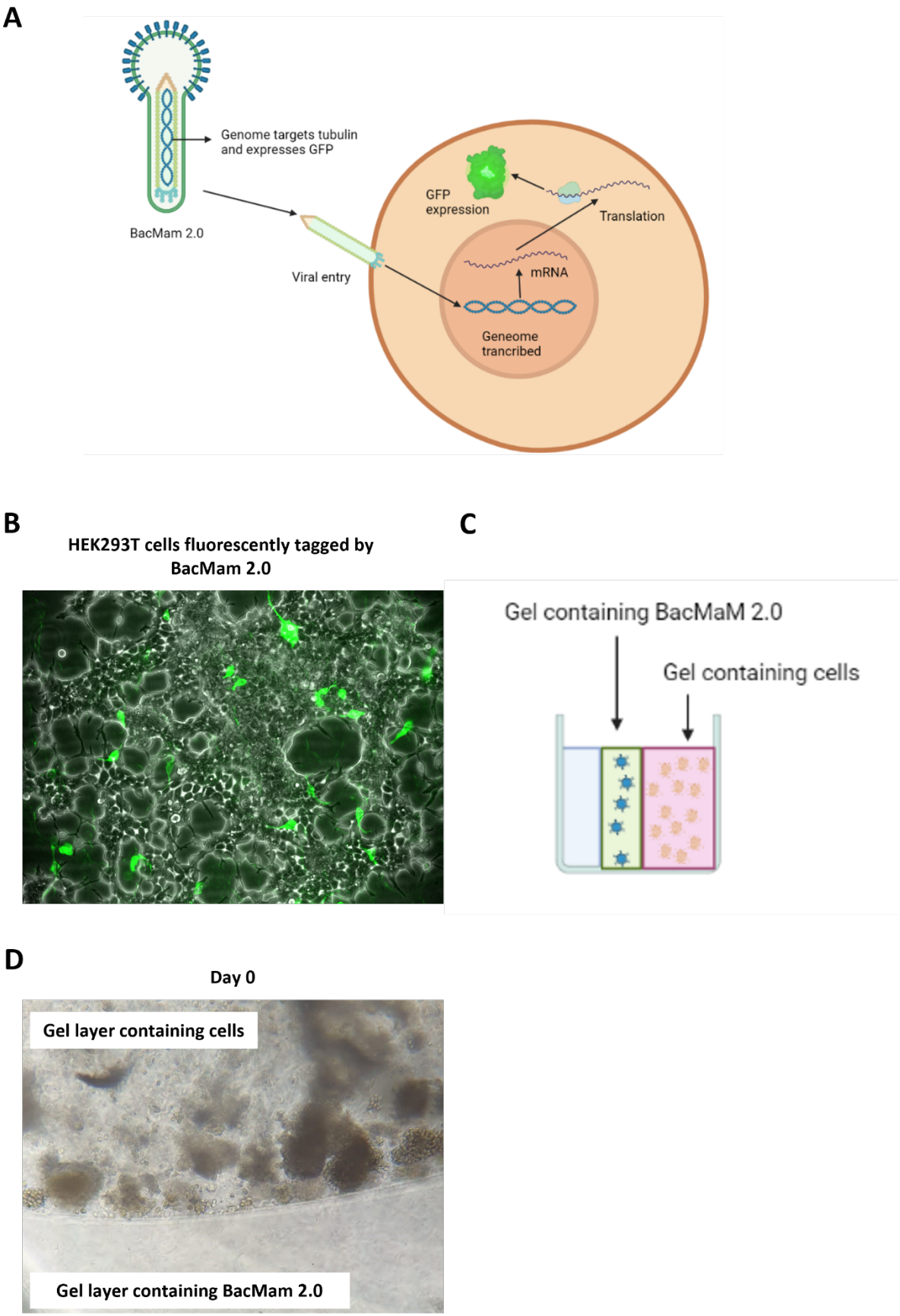

Figure 5: Determining if BacMam 2.0 is an appropriate method to distinguish migrating cells from non-migrating cells. A. The BacMam 2.0 technology utilises an insect baculovirus as a vehicle to transduce a human tubulin construct fused with emGFP

to fluorescently tag cells (Created using Biorender.com). **B.** HEK293T cells cultured in DMEM medium were exposed to the BacMam 2.0 and show that the tagging method is functional. **C.** Schematic diagram showing the set-up of the vertical layer system (Created using Biorender.com). **D.** After preparing the first invasion assay set-up, the cells encapsulated in one layer were evidently separated from the gel layer containing BacMam 2.0.

As our initial method did not meet the required standards for further analysis, we tested three additional set-ups: 1. Performing the invasion assay in 8-chambered slide, 2. Performing the invasion assay in an angiogenesis slide, and 3. Creating slices in the gel matrix (**Appendix 1C**) (**Figure 6**). The aim of these approaches was to identify an optimal set-up that would result in the clear discernment of migrating HSDJ-DIPG-07 cells from non-migrating cells. The 8-chambered slide set-up utilised the BacMam 2.0 technology to fluorescently tag cells that invaded into adjacent layers, as well as a secondary antibody that was hypothesised to make visualisation of the separate layers more definite (**Figure 6A**). The angiogenesis slide approach similarly utilised the BacMam 2.0 technology, however thinner bioscaffold layers were used to theoretically distinguish even the cells that were only able to migrate very short distances (**Figure 6B**). The final approach incorporated the BacMam 2.0 into the entire gel, and only required cells to be seeded into a slice created by a scalpel (**Figure 6C**). This approach was hypothesised to diminish the visualisation issues associated with gel layers. Despite these hypothesised novel approaches, the BacMam 2.0 remained inactive, making it difficult to distinguish between migrating and non-migrating populations. Furthermore, it was difficult to distinguish between cell populations because of background interference of cells at different depths in the gel as well as difficulties in distinguishing between layer boundaries. Therefore, it was evident that the BacMam 2.0 technology was not suitable for use in both HSHP and Matrigel, and the usage of different gel layers additionally created hurdles for visualisation of cells.

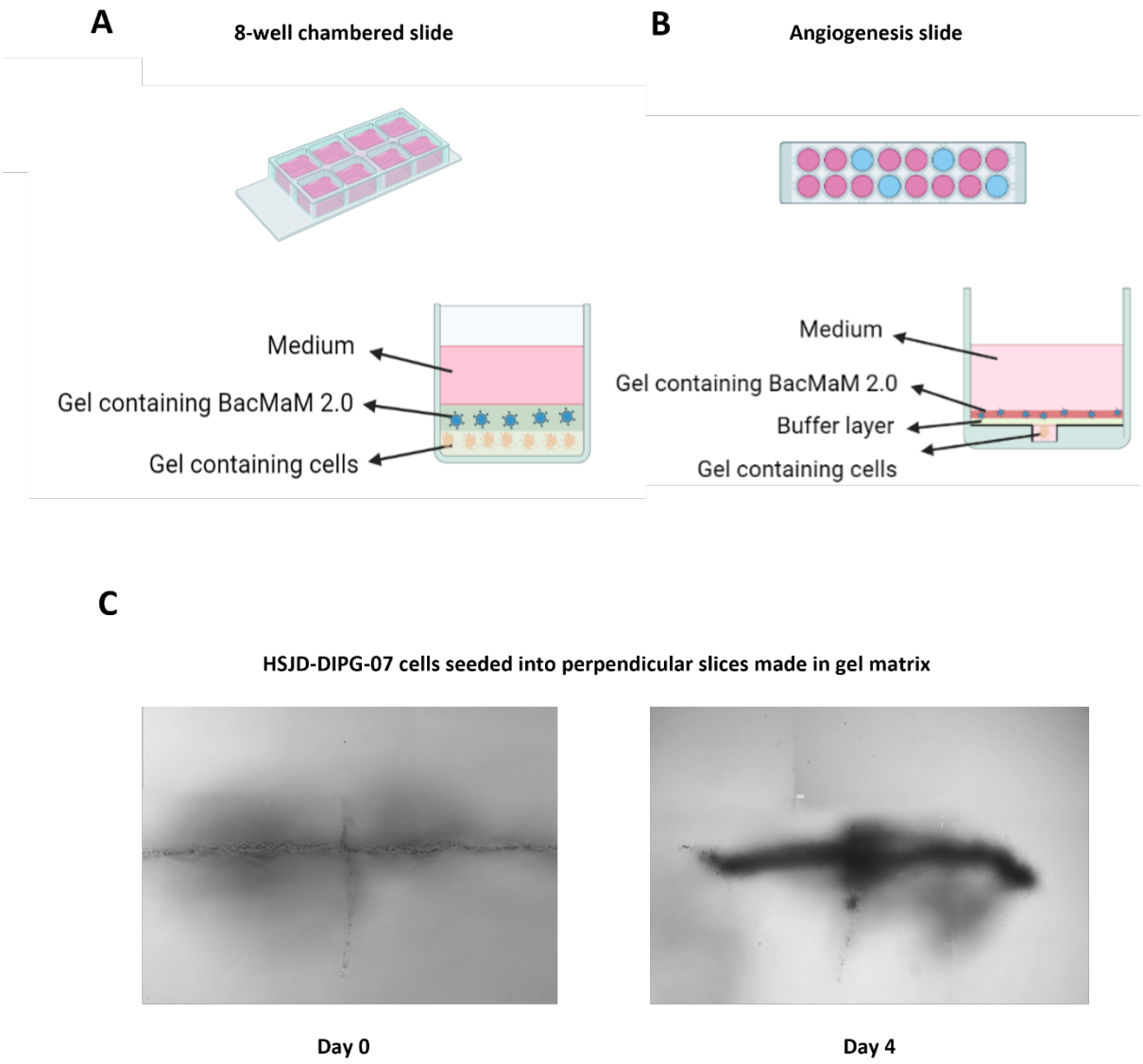

Figure 6: Different approaches aimed at improving the discernment of migrating cells from non-migrating cells in the invasion assay. A. Illustration of the 8-chambered slide set-up including the different layers of gel used (Created using Biorender.com). **B.** Illustration of the angiogenesis slide set-up including the thinner layers of gel included (Created using Biorender.com). **C.** A scalpel was used to make perpendicular incisions into the HSHP matrix. The cells were visualised at day 0 and day 4.

The previous invasion assay approaches were limited by difficulties associated with distinguishing invading and non-invading cells. To overcome this limitation, an invasion assay prototype (**Figure 7**) was developed in collaboration with Professor Monique den Boer using PDMS mould (**Figure 7A**). IUE-24B7 murine cells were chosen for acquiring the proof-of-concept data because of their GFP positivity and because of their future use in CRISPR-KO screening. The IUE-24B7 murine cells were seeded together with Matrigel into one circle and monitored for 8 days to determine their ability to invade into the next circle containing Matrigel **(Figure 7B)**. The imaging results show that IUE-24B7 cells require the formation of dense networks between single cells, thus migrating away from the bridge towards a 'denser' cell area. Interestingly, the PDMS invasion assay approach could be used for 3D imaging, as the

material was auto fluorescent and clearly outlined the boundaries of the invasion area, whilst allowing individual cells to be distinguished in a Z-stack of different depths (**Figure 7C**). Overall, several observations were made when using the PDMS invasion assay prototype: (1) The PDMS invasion assay prototype has the potential to be a suitable approach to distinguish migrating and non-migrating cells (if we can get the cells to cross the 'bridge'). (2) The cells remain viable in the invasion assay even after 8 days. (3) The PDMS invasion assay prototype is also suitable for 3D imaging techniques. (4) The large area of the circles means that the cells need to cover large distances to visibly invade into the empty gel.

To overcome the limitation of cells having to invade large distances to be considered 'invading', a drop invasion assay, inspired by the PDMS mould approach, was attempted (**Figure 8**). The drop invasion assay consisted of creating two 'bubbles' of Matrigel on a glass cover slide and connecting the drops with a 'bridge' of cells (**Figure 8A**). The invasion of cells was monitored over the course of 12 days (**Figure 8B, 8C**), and the average total invasion distance was quantified (**Figure 8D**). From the imaging results, t is evident that the cells are capable of invading into the drops of gel. As it is known that the circular drops of gel initially contained no cells, it is easy to distinguish invading and non-invading cells. Furthermore, the results confirmed that seeding the cells into the confined 'bridge' section allowed cells to form a dense network and promote cell invasion, unlike what was observed in **Figure 7C**. Therefore, the results show that the drop invasion assay is a feasible and effective method for visualising the invasive capabilities of cell *in* vitro.

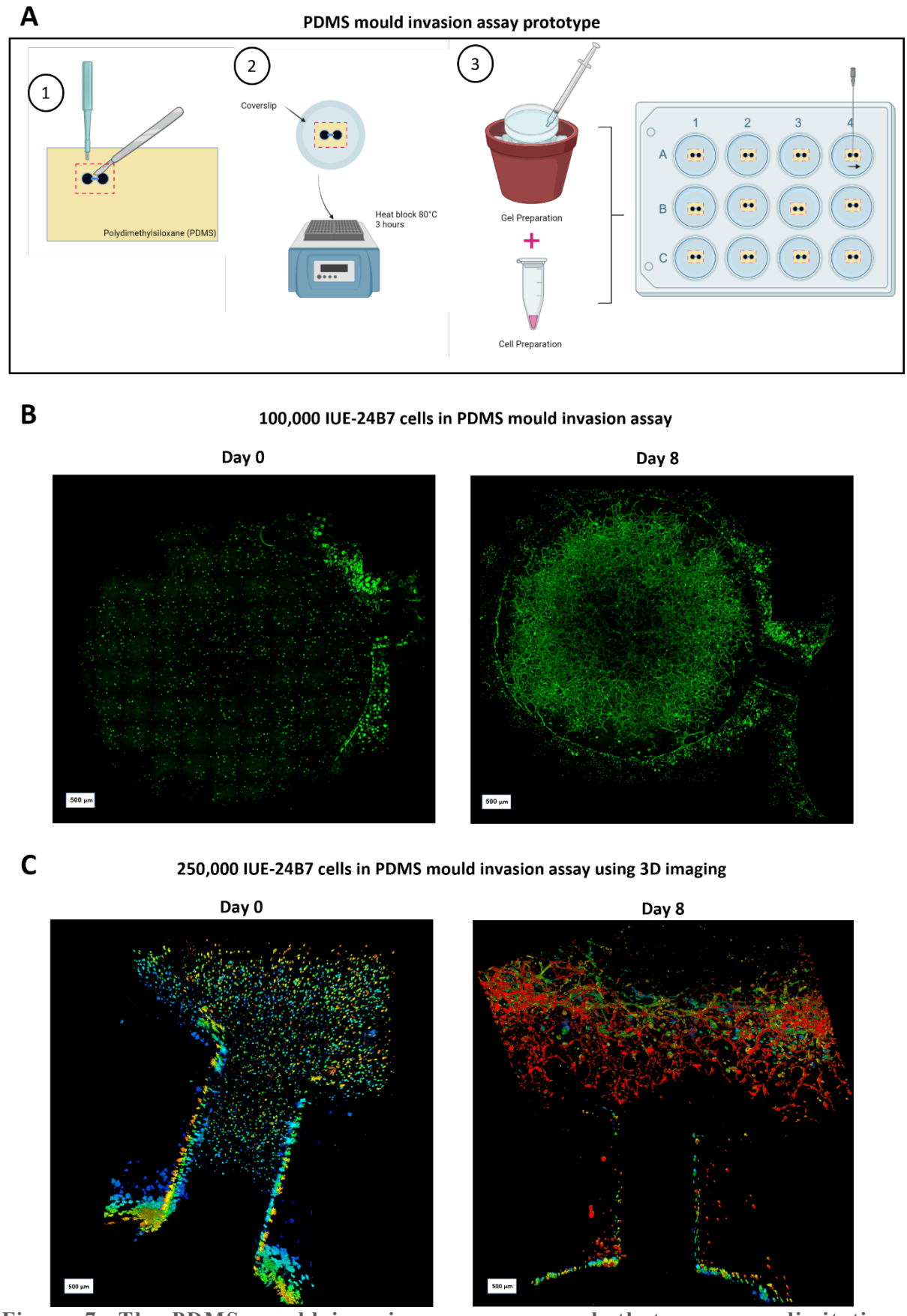

Figure 7: The PDMS mould invasion assay approach that overcame limitations associated with distinguishing invading and non-invading cells. A. Illustration providing an overview of how the PDMS mould invasion assay prototype was set-up. (1)

A scalpel and biopsy puncture were used to cut out two circles connected by a bridge from PDMS mould. (2) The punctured PDMS mould was placed on a coverslip and left to adhere on a hot plate. (3) The gel and cells were prepared and seeded into the PDMS mould (Created using Biorender.com). **B.** Fluorescent imaging showing the behaviour of 100,000 IUE-24B7 cells (in green) after being seeded into the PDMS mould invasion assay on day 0 and day 8. **C.** 3D imaging of 250,000 IUE-24B7 cells seeded into the PDMS mould invasion assay on day 0 and day 8. The cells retreated to the area with higher cell density by day 8. The different colours represent cells at different depths in the gel.

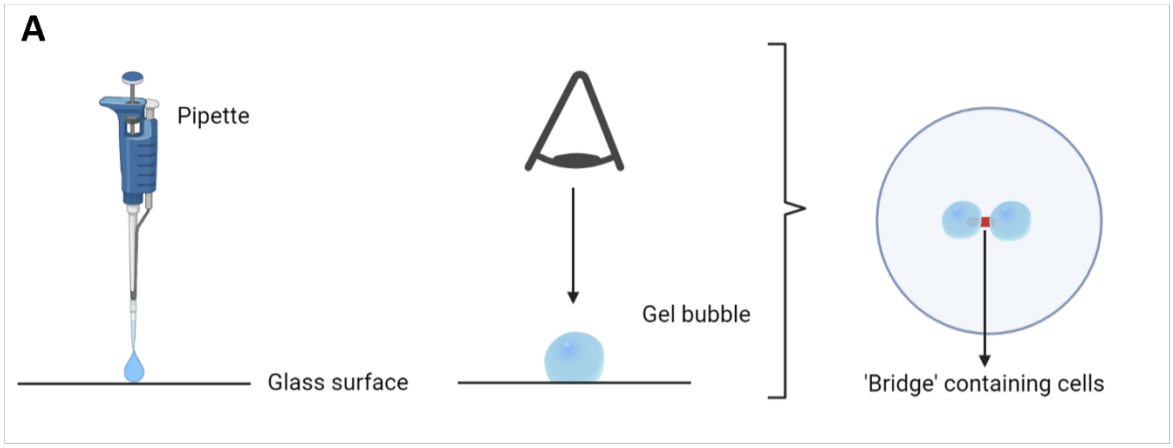

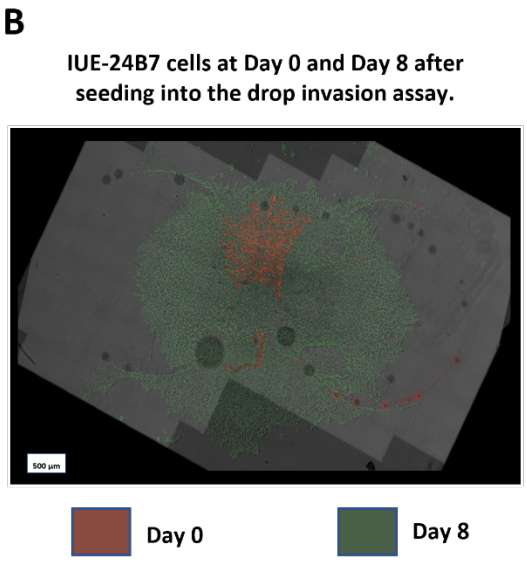

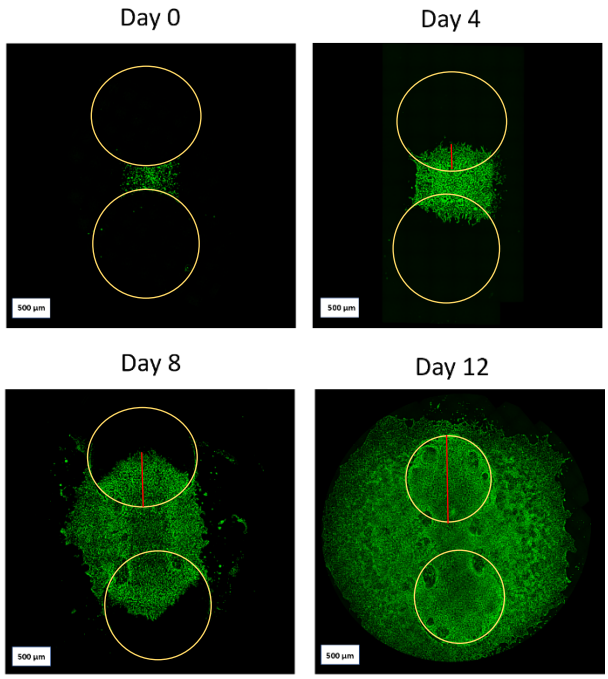

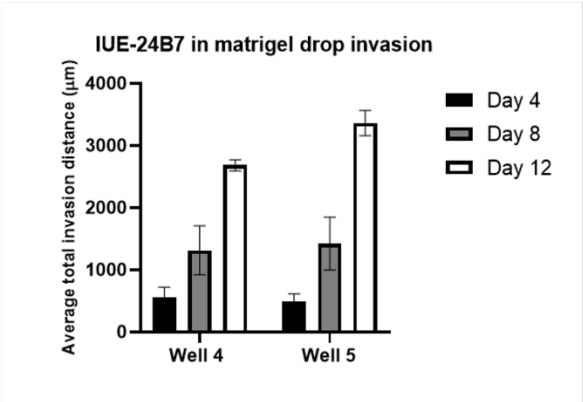

Figure 8: Seeding cells into the bridge of the drop invasion assay allowed IUE-24B7 to invade into the empty circles. A. Illustration showing how the drop invasion assay was set-up. The 10,000 IUE-24B7 cells were seeded into the 'bridge' section connecting two circles of empty gel (Created using Biorender.com). **B.** An overlay of the drop invasion assay images showing the position of cells at day 0 (red) and day 8 (green). **C.** Images of the drop invasion assay at day 0, day 4, day 8 and day 12. The yellow circles illustrate the boundaries of each drop. The red line illustrates the invasion distance. **D.** Bar graph quantifying the average total invasion on day 0, day 4, day 8 and day 12 (n=1).

Establishing CRISPR-Cas9 Knockout Screens in pHGG and ATRTs

For uncovering novel therapeutic targets, it is vital to identify the genes involved in pHGG and ATRT invasion. To achieve this, CRISPR-KO screens were implemented into a variety of primary patient derived pHGG and ATRT cells, and *intra utero* established murine DMG cultures **(Figure 9)**. The first step of CRISPR-KO screening was to stably introduce a doxycycline inducible *Cas9* gene into the genome of the target cells using lentiviral transduction. The doxycycline inducible Cas9 allows us to control Cas9 activation and therefore limit any off-target effects and DNA damage caused by constitutively active Cas9. Lentiviruses carrying a GFP-coding gene were used as positive controls, to determine transduction timing and efficiency of the method **(Figure 9A)**. Once ready, the transduced cells were selected with either puromycin or blasticidin before performing western blots to determine if the transduction was successful **(Figure 9B)**. The doxycycline inducible Cas9 construct is controlled by a TET-on promoter that relies on the presence of doxycycline to induce expression of the Cas9 protein. Using western blotting, we found that most cell lines were successfully transduced, except for VUMC-ATRT-01 pCW-Cas9 blast, OBPG-DIPG-02 pCW-Cas9 blast and 26C2 pCW-Cas9 blast. As expected, increasing the concentration of doxycycline also increased the expression of pCW-Cas9 in the transduced cells. Especially with cells transduced with the pCW-Cas9 blast construct, bands were visible for both the control and the doxycycline-induced groups, suggesting that the pCW-Cas9 blast construct was 'leaky'. To eliminate the possibility that the pCW-Cas9 blast construct was being constitutively activated by antibacterial components in the media, the same cells were cultured in different media prior to western blotting **(Figure 9C)**. The western blot revealed that even though there is increased expression of pCW-Cas9 blast in the presence of doxycycline, there remains constant activation of pCW-Cas9 blast in the absence of doxycycline with or without antibiotics. With these results, we were able to conclude which constructs had been successfully transduced and that the pCW-Cas9 blast was 'leaky'.

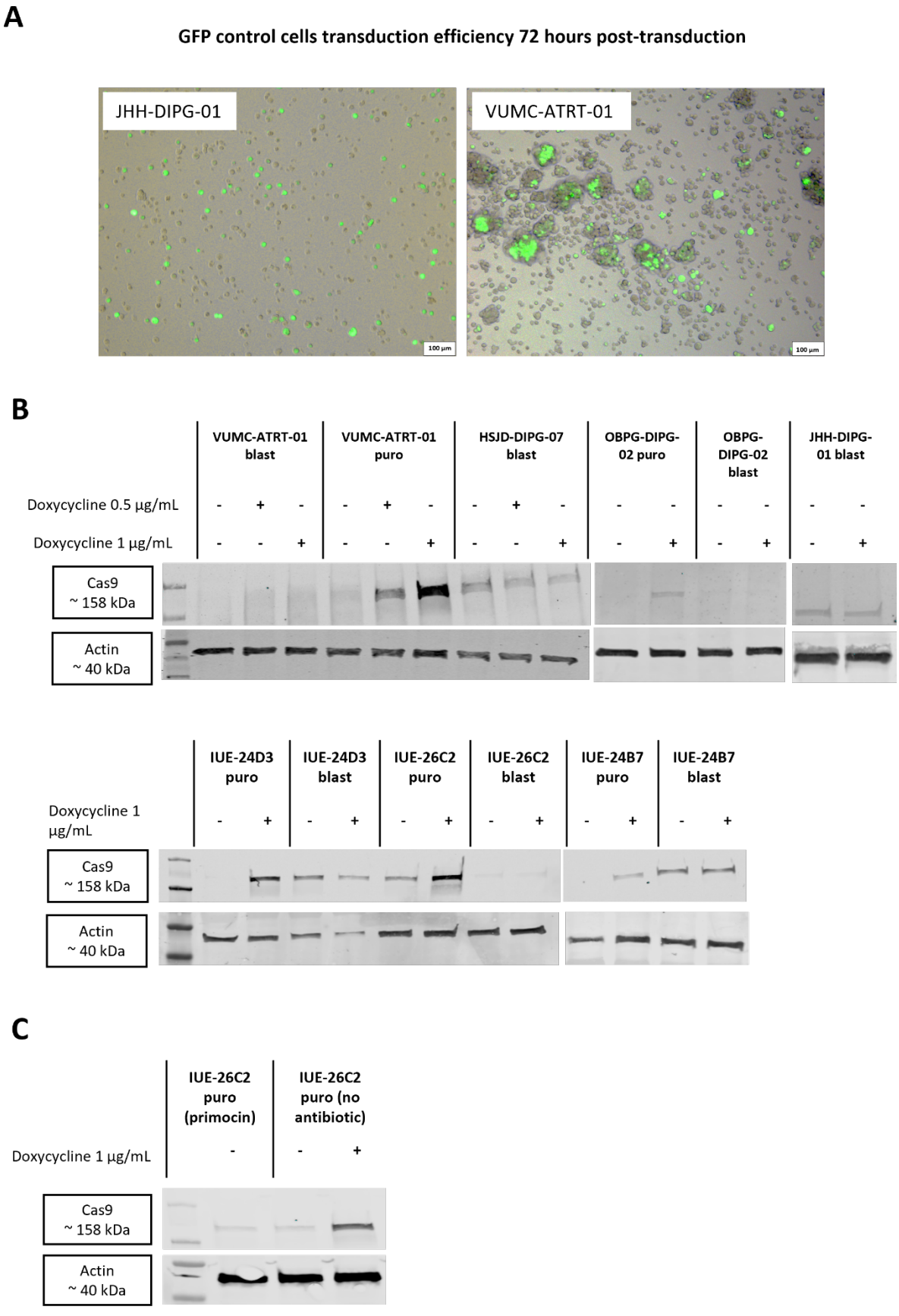

Figure 9: pCW-Cas9 puro was successfully transduced in some cell lines whilst pCW-Cas9 blast appears to be a leaky construct. A. GFP fluorescent control cells after

transduction with pHIV-EGFP **B.** Western blots showing the outcome of the transduction procedure of several cell lines following 1 week selection on either puromycin or blasticidin. The control groups were not exposed to doxycycline. **C.** To determine if the leakiness observed in the pCW-Cas9 blasticidin construct was the result of Cas9-induction by the antibiotics in the medium, a western blot was performed in the 26C2 pCW-Cas9 puro cell line cultured in different media for 1 week.

The second step of the CRISPR-KO screening involved performing another transduction on pCW-Cas9 cells. A CRISPR library, containing a pool of sgRNAs that will guide the Cas9 endonuclease to specific genes in the genome, was transduced into pCW-Cas9 cells. However, before performing the transductions, we validated the distribution of the sgRNAs in the CRISPR screen libraries, ensuring that all the sgRNAs are represented evenly to prevent any result bias. Therefore, a deep sequencing analysis was performed on the human kinome library, the human nucleosome library, and the mouse kinome library **(Figure 10)**. The CRISPR library v1 was sequenced by Addgene (Addgene.com) and only information about the sgRNA read count distribution is provided. The distribution of the read counts provides valuable information about skewing of the library (**Figure 10A & 10B**). According to the sequencing results, the human kinome library contains 2582 sgRNAs that are normally distributed, with the majority of sgRNAs with 200 -500 read counts per guide **(Figure 10A-1)**. This suggests that there is a good representation of each sgRNA in the library. Similarly, the mouse kinome library, which contains 2659 sgRNAs, also appeared to have an even distribution of sgRNAs with between 500 – 1000 read counts per sgRNA **(Figure 10A-3)**. As both the human kinome library and mouse kinome library both have more than 80% of successfully mapped reads with only a few zero counts, it was concluded that most, if not all, genes are accounted for in the respective libraries. Conversely the human nucleosome library, which contains 37,330 sgRNAs, appeared to be severely skewed, with 2515 sgRNAs with zero counts and a very uneven distribution of guides **(Figure 10A-2)**. The very broad peak in the **Figure 10A-2** conveys that the majority of sgRNAs have between 4 and 64 read counts per guide, a 15-fold difference in sgRNA representation between most guides. The overrepresentation of some sgRNAs is also confirmed by the relatively high Gini index, which is commonly used in economics to measure income inequality and suggests that the distribution of sgRNAs represented in the nucleosome library is uneven **(Figure 10B)**.[66] Using the human nucleosome library for CRISPR screens would mean that the overrepresented sequences would dominate the data and therefore skew the results. Finally, the 77,406 sgRNAs in the CRISPR library v1 appear to have a chi-squared distribution, suggesting that there will be some overrepresented sgRNAs, however this is not as severe as what is expected with the human nucleosome library **(Figure 10A-4)**. The graph in **Figure 10A-4** shows that the majority of sgRNAs are represented at a low frequency, between 1 and 8 read counts, and therefore it is possible that some genes may not be represented in the CRISPR pool following library transduction. Despite this, it was concluded that the human kinome library, mouse kinome library and human lentiviral CRISPR library v1 were all suitable for future CRISPR-KO screening.

A

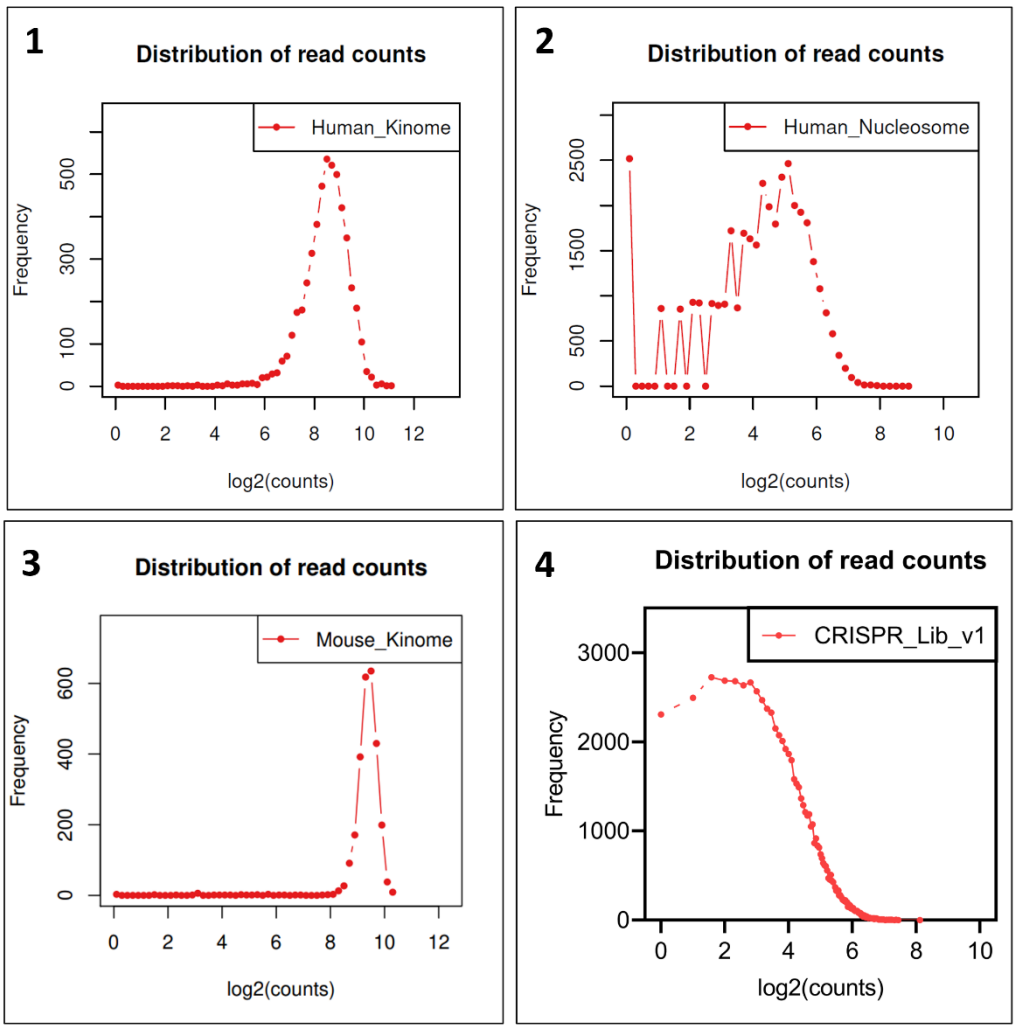

B

Library	Reads	Mapped	Percentage	Total sgRNA	Zero counts	Gini Index
Human Kinome	2378811	2069361	86.99	5070	2	0.05641
Human Nucleosome	1250784	960417	76.79	37330	2515	0.2273
Mouse Kinome	2210352	1796521	81.28	2659	3	0.02607

Figure 10: Validation of sgRNA distribution. **A.** Graphs depicting the distribution of sgRNA counts. **B.** A table summarising the deep sequencing data. The table also quantifies the number of zero counts and the Gini index, which measures the evenness of sgRNA read counts.

Given that the transduced cell lines being prepared are to be used for CRISPR screens, cell lines containing leaky constructs were discarded. The pHGGs transduced with pCW-Cas9 puro, however, were suitable for combination with blasticidin resistant CRISPR libraries such as the Human kinase CRISPR-KO library. Since the genome wide CRISPR-KO libraries to be used in combination with the ATRTs are puromycin resistant, a different Cas9 construct was transduced into the ATRT cells in preparation for CRISPR screening. The VUMC-ATRT-01 and VUMC-ATRT-03 were transduced with a pCW-Cas9-2A-EGFP construct, a doxycycline

inducible Cas9 construct that also expresses GFP under the same promoter **(Figure 11)**. As a control, GFP-coding lentivirus was used to determine the transduction efficacy **(Figure 11A)**. Next, pCW-Cas9-2A-EGFP transduced cells were exposed to 2 μg/mL doxycycline for 24 hours before being sorted using FACS based on GFP positivity **(Figure 11B)**. Surprisingly, our FACS results only showed a single peak when analysing the pCW-Cas9-2A-EGFP cells, indicating a 100% transduction efficiency. This was unexpected because from previous experience where we had seen two distinct peaks in the histograms, representative of a transduced cell population and an untransduced cell population. Therefore, to verify these results we performed another FACS analysis using untransduced VUMC-ATRT-03 cells exposed to doxycycline, to determine if doxycycline has autofluorescence properties **(Figure 12)**. Our FACS analysis revealed that doxycycline is indeed auto fluorescent. As a result, we concluded that the transduction of pCW-Cas9-2A-EGFP in VUMC-ATRT-01 and VUMC-ATRT-03 had failed.

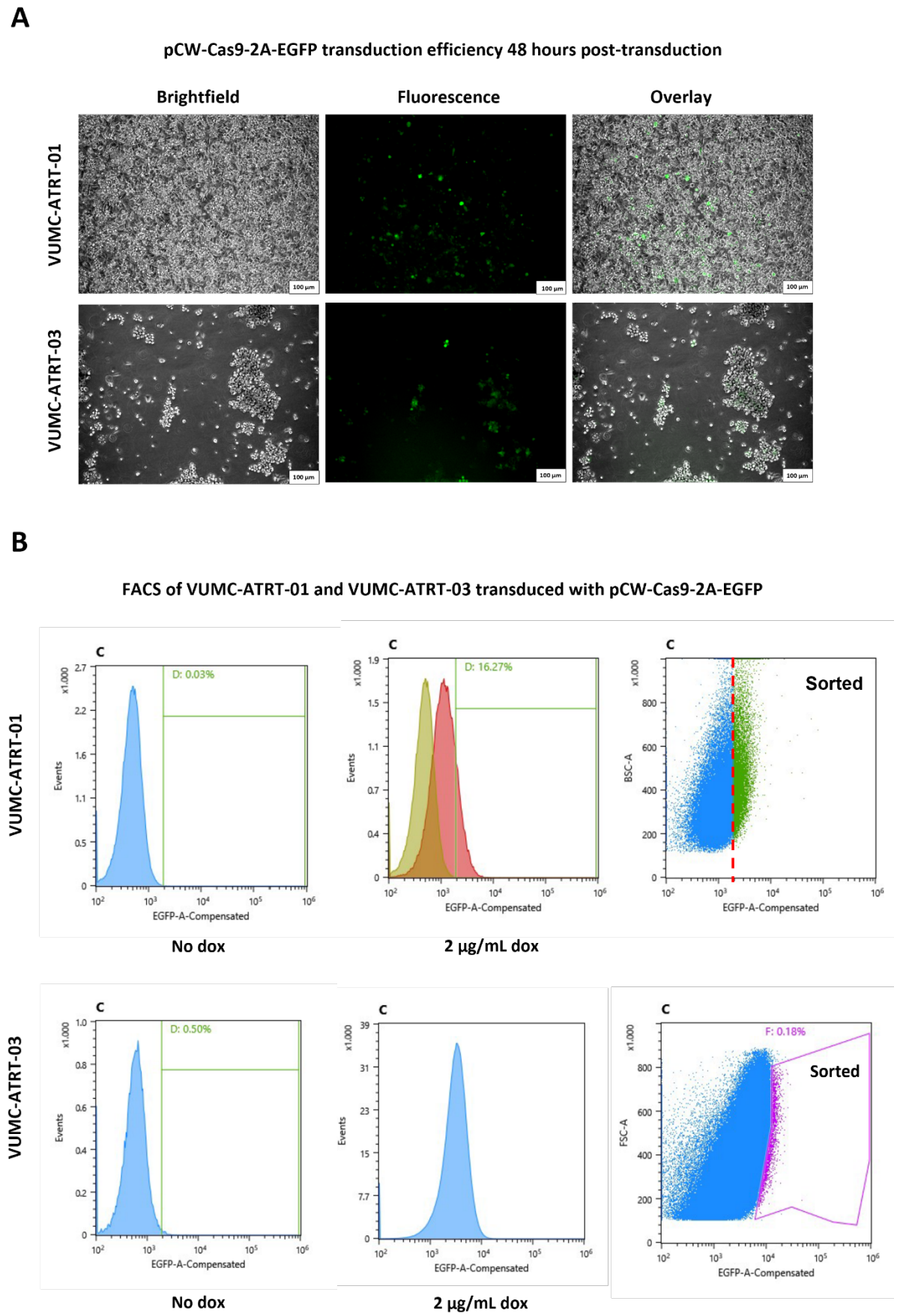

Figure 11: VUMC-ATRT-01 and VUMC-ATRT-03 cells were transduced with pCW-Cas9-2A-EGFP. A. The transduction efficiency can be visualised using pHIV-EGFP

construct groups. **B.** The FACS panel of the sorting and gating of transduced VUMC-ATRT-01 and transduced VUMC-ATRT-03 cells. The green peak in the transduced VUMC-ATRT-01 panel represents GFP emission of transduced cells not exposed to doxycycline.

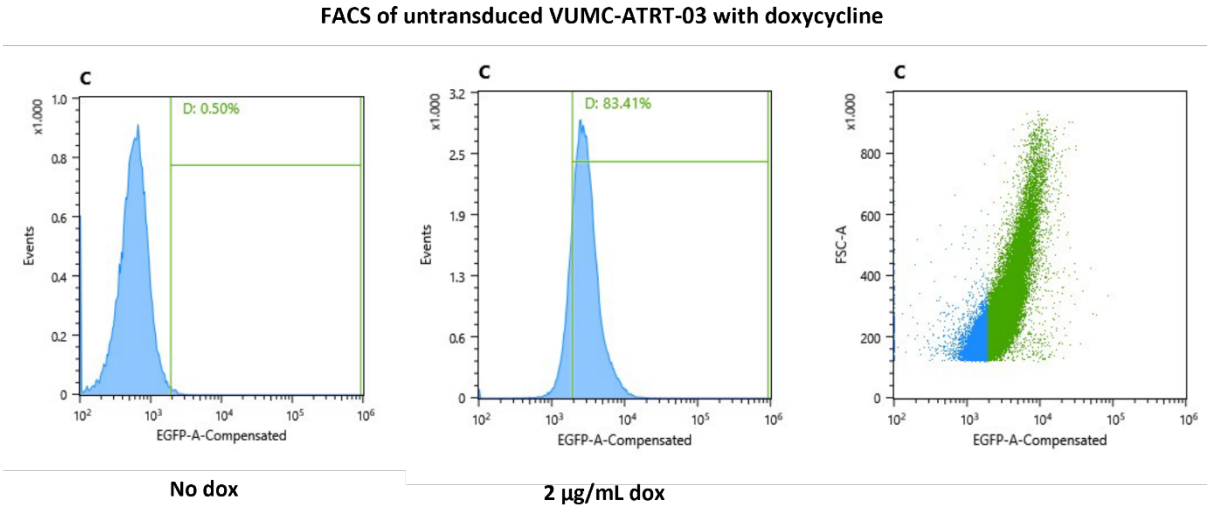

Figure 12: Doxycycline is auto fluorescent. The FACS panel of untransduced VUMC-ATRT-03 exposed to doxycycline. The gating shown was the same gating used for the cell sorting procedure in transduced cells.

Seeing that only the pCW-Cas9 puro construct was successfully transduced into the ATRT cell lines, we decided to use a genome wide CRISPR-KO library that could be selected based on GFP positivity instead of puromycin. The Human lentiviral CRISPR library v1 was a suitable library to combine with ATRT Cas9-puro cell lines **(Figure 13)** because often ATRT have a disrupted BBB that somewhat enhances drug delivery, therefore allowing the elucidated molecular targets to become more accessible than in pHGGs.[67,68] Firstly, western blotting was performed on VUMC-ATRT-01 and VUMC-ATRT-03 exposed to doxycycline to determine if the pCW-Cas9 puro transductions were successful **(Figure 13A)**. The western botting results show that the VUMC-ATRT-03 expressed Cas9, however, the transduction of the VUMC-ATRT-01 had failed. The library transduction was therefore only performed in VUMC-ATRT-03 pCW-Cas9 puro cells. These cells had undergone multiple puromycin selection rounds to ensure that all remaining cells carry the pCW-Cas9 construct. As the Human lentiviral CRISPR library v1 is fluorescently tagged with GFP, the transduction efficiency could be visualised using fluorescent microscopy **(Figure 13B)**. Following a one-week recovery period, a FACS procedure was followed for the transduced VUMC-ATRT-03 pCW-Cas9 puro cells and 2.65% of these cells were successfully sorted, equating to 14 million cells and a x200 initial coverage of all sgRNAs **(Figure 13C)**. The cells were expanded for future experiments **(Figure 13D)**.

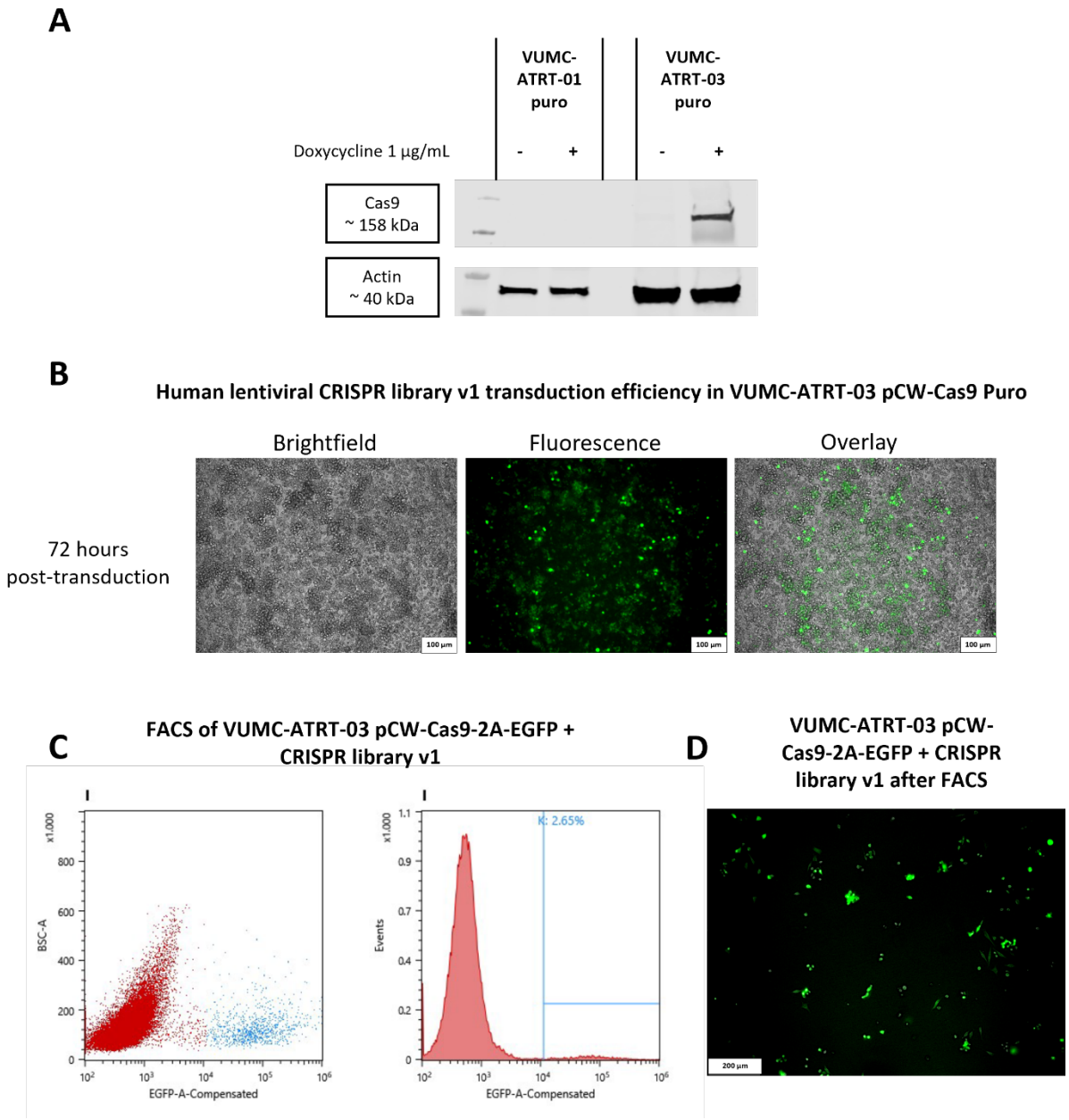

Figure 13: CRISPR library v1 was successfully transduced into VUMC-ATRT-03 pCW-Cas9 puro cells. A. A western blot confirming the presence of Cas9 protein in VUMC-ATRT-01 and VUMC-ATRT-03 cells. **B.** Fluorescent imaging depicting the transduction efficiency of CRISPR library v1 in VUMC-ATRT-03 pCW-Cas9 puro cells. **C.** FACS panel showing the gating and percentage of sorted cells (2.65%). **D.** Fluorescent imaging showing the population of VUMC-ATRT-03 pCW-Cas9 puro + CRISPR library v1 cells 5 days post-FACS.

Discussion

The highly invasive phenotype of pHGG and ATRT and its implications on therapeutic response is widely acknowledged; and although there are many well established invasion assay approaches used to visualise cell invasion *in vitro*, there remains no assay to identify the molecular drivers of cell invasion in a high-throughput approach.[18,69] To this end, we tested different invasion assay set-ups that can be combined with established CRISPR-KO screens to identify the molecular drivers for pHGG and ATRT invasion. Through testing different *in vitro* invasion assays, we show that the drop invasion assay was the most promising system tested, where we were able to clearly distinguish the invading and non-invading cells over time. Additionally, utilising lentiviral transductions, western blots and FACS, we show the feasibility of performing CRISPR-KO screens in primary patient-derived pHGG and ATRT cultures. Together, these findings provide the foundation for investigating the effect of genome-wide perturbations on the invasive behaviour of pHGG and ATRT, potentially revealing novel druggable targets to supress invasion *in vivo*.

Testing different invasion assay set-ups has demonstrated the role the tumour microenvironment composition plays in influencing tumour cell invasion. In this study, our utilisation of both Matrigel and HSHP as bioscaffolds for the spheroid invasion assays with pHGG cell cultures revealed the inhibitory effect of HSHP on tumour cell invasion. Theoretically, its comparable HA content and adjustable stiffness and pore size made the HSHP matrix an attractive candidate for modelling the brain-tumour microenvironment.[70,71] However, when testing the HSHP bioscaffold we found that cells were unable to invade the matrix. Similar findings were also described by Lan *et al.* (2016), who showed that cross-linked HA gel (CHAG) inhibited gastric and hepatic tumour cell invasion.[72] It was hypothesised that the sticky nature of CHAG limited the interaction between known motility receptors, such as CD44 or RHAMM, and their stimulating molecules by physically wrapping around the cells.[72] This would also explain the inhibitory effect witnessed with the HSHP matrix, which likewise is sticky. Alternatively, the HA polymer length has been shown to influence the invasive behaviour of tumour cells and may have been responsible for the outcomes observed in this study.[73] Whilst Tan *et al.* (2011) showed that LMW-HA promoted the invasive phenotype of human breast cancer cells, Tian *et al.* (2013) showed that cancer resistance in naked mole-rats is mediated by elevated high molecular weight HA (HMW-HA) that interacts with CD44 receptors to inhibit malignant behaviours.[74,75] Using this knowledge, we can alternatively hypothesise that the HSHP matrix contains HMW-HA that inhibited tumour cell invasion; however, further research into the subject would be necessary to confirm the hypothesis. Evidently, we showed that the choice of bioscaffold largely influences invasion outcomes, emphasising the importance of mimicking the brain-tumour microenvironment to obtain relevant results *in vitro*.

In addition to the choice of bioscaffold, we show that the structure of the invasion assay also influences the invasive behaviour of tumour cells. When testing the PDMS mould method, we showed that the IUE-24B7 cells migrated away from the ‘bridge’ and towards the area denser in cells. A similar behaviour was also described by Zanotelli *et al.* (2019), who showed that

human breast cancer cell lines in Y-shaped microtracks preferentially chose the wider paths to minimise energy costs.[76] This migration-decision making theory suggests that tumour cell invasion is directly correlated to physical confinement and steric hinderance, where cells will invade the 'path of least resistance' to avoid the high energy expenditure associated with invading through confined spaces.[76] Taken together, our results show the impact the layout of the invasion assay has on influencing cell invasion *in vitro*, and further suggests the importance of designing an invasion assay that mimics the decision-making scenarios encountered by tumour cells *in vivo*.

The second component of this project was to establish CRISPR-KO screens in different primary patient derived pHGG and ATRT tumoroids that could later be incorporated into the invasion assay. To achieve this, we first had to transduce the cells with a doxycycline inducible Cas9 construct. A doxycycline inducible Cas9 construct was used because the timing of Cas9 activation can have a significant impact on the results obtained from the CRISPR-KO screen.[57] With constitutively activated Cas9, cells transduced with sgRNAs targeting essential genes such as *MYC* would be rapidly depleted because of immediate cell death.[77] Therefore, with a doxycycline inducible Cas9 system we can temporally control Cas9 expression, and thus the early time point effects of a perturbation can still be observed in the CRISPR-KO screen.[57]

Moreover, the use of a doxycycline inducible Cas9 system can prevent further skewing of sgRNA distribution before day 0 of the CRISPR-KO screen. For this project, we used the CRISPR library v1. Analysis of the sgRNA read counts and distribution revealed that the majority of the 77,406 sgRNAs have between 1 and 8 counts per a guide. On average, literature has recommended that each sgRNA should have between 300 – 500 read counts to be sufficiently represented in a library.[57,66] Sufficient representation plays a crucial role in the statistical power of downstream analysis because it may be difficult to correctly determine the statistical significance of a genetic perturbation with such a low representation in the library. However, because the library validation was performed before transducing the pooled library into the cells, it is expected that following library transduction and expansion in the cells, that the representation of each sgRNA will also increase, recovering the statistical power. Instead, we believe that the distribution of the sgRNAs is a more important measure for CRISPR library validation because an uneven distribution results in the overrepresentation of certain sgRNAs that will have an impact on downstream analysis. We show that the CRISPR v1 library has a chi-squared distribution and therefore we expect that some sgRNAs will be overrepresented in the cell population. However, by acquiring the sgRNA read count and distribution at day 0, we can normalise the data for later points and therefore account for the overrepresentation of certain sgRNAs. Together, we used the library validation to determine the suitability of the CRISPR v1 library and showed how we can overcome the limitations associated with the low sgRNA read counts and chi-squared distribution.

This study has three main limitations. The first limitation is the scalability of the drop invasion assay. To be combined with a genome-wide CRISPR-KO screen, at least 40 million cells containing the transduced CRISPR constructs need to be placed in the invasion assay. Given that approximately 10,000 cells are used for a single drop invasion assay, the current approach

would require approximately 4,000 individual assays to reach the volume of cells required for *in vitro* CRISPR-KO screening. This makes the drop invasion assay impractical to perform manually and it is therefore necessary to adapt the method for high throughput applications. For large institutions, the simple set-up of the drop invasion assay could allow for automation of the approach, reducing the workload for the researcher. Alternatively, the drop invasion assay could be adapted so that a larger volume of cells can be seeded into a single assay. One example of such adaptions is to pipette two elongated columns of bioscaffold 1mm apart onto a glass slide, with the cells sandwiched in between the columns. In this way, the drop invasion assay can be adapted for high-throughput applications. The second limitation is that sometimes cells would 'crawl' over the surface of the invasion assay, rather than invade through the bioscaffold. This behaviour of choosing the 'path of least resistance' is anticipated for invading cells, and our study overcame this limitation by performing Z-stacks when imaging cell invasion *in vitro*. By doing so, truly invading cells were recognized from crawling cells, an important distinction to make because of the differences in underlying biological processes regulating these mechanisms. The final limitation of this study is the low transduction efficiency used for transducing the CRISPR library into Cas9-expressing cells. Given that it is necessary that only one sgRNA is incorporated into a single cell, we aim for an MOI (multiplicity of infection) of 0.3 to limit the chances of multiple perturbations in a single cell. However, to achieve a x250 coverage of the sgRNA library with a 3% transduction efficiency would mean that ideally 600 million cells need to be transduced. This large volume of cells requirement makes it difficult to perform genome-wide CRISPR screens on slow-growing cell cultures. Nevertheless, we strongly believe that using a low MOI is important for ensuring that only one sgRNA is introduced per a cell.

In the future, it is necessary to further optimise the invasion assay by identifying or developing a suitable bioscaffold that mimics the brain-tumour microenvironment. Recently, Wang *et al.* (2022) described a novel matrix that mimics both brain stiffness and tumour microenvironment. The brain-stiffness-mimicking gel is composed of collagen I, Matrigel and HA and therefore contains components that model the basement membrane, as well as the high HA content resembling the brain parenchyma.[78] Furthermore, incorporating other components such as microglia and astrocytes to model cellular interactions would enhance *in vitro* tumour microenvironment modelling, potentially improving the reliability of results obtained from the invasion assay because tumour-microenvironment interactions have been shown to play an important role in tumour invasion *in vivo*.[79]

In conclusion, this research project provided the foundation for performing *in vitro* invasion assays combined with high-throughput CRISPR-KO screens. Although future work will be needed to further elucidate the molecular drivers of pHGG and ATRT invasion, our findings could shed light on promising targets that can hinder the invasive capabilities of pHGG and ATRT and therefore improve the effectiveness of current therapeutic strategies by confining the tumour cells to their area of origin. Furthermore, the findings elucidated in this study are not restricted to a single tumour subtype and can potentially be applied to all invasive tumours. Ultimately, this study has contributed to improving the treatment outcomes of thousands of patients suffering from invasive tumour diseases.

References

(1) Udaka, Y. T., & Packer, R. J. (2018). Pediatric Brain Tumors. Neurologic Clinics, 36(3), 533-556. doi:https://doi.org/10.1016/j.ncl.2018.04.009

(2) Jacques, G., & Cormac, O. (2013). Chapter 99 - Central nervous system tumors. In O. Dulac, M. Lassonde, & H. B. Sarnat (Eds.), Handbook of Clinical Neurology (Vol. 112, pp. 931-958): Elsevier.

(3) Fangusaro, J. (2012). Pediatric high grade glioma: a review and update on tumor clinical characteristics and biology. Front Oncol, 2, 105. doi:10.3389/fonc.2012.00105

(4) Hakar, M. H., & Wood, M. D. (2020). Updates in Pediatric Glioma Pathology. Surg Pathol Clin, 13(4), 801-816. doi:10.1016/j.path.2020.08.006

(5) Ferris, S. P., Hofmann, J. W., Solomon, D. A., & Perry, A. (2017). Characterization of gliomas: from morphology to molecules. Virchows Archiv, 471(2), 257-269. doi:10.1007/s00428-017-2181-4

(6) Louis, D. N., Perry, A., Wesseling, P., Brat, D. J., Cree, I. A., Figarella-Branger, D., . . . Ellison, D. W. (2021). The 2021 WHO Classification of Tumors of the Central Nervous System: a summary. Neuro-Oncology, 23(8), 1231-1251. doi:10.1093/neuonc/noab106

(7) Braunstein, S., Raleigh, D., Bindra, R., Mueller, S., & Haas-Kogan, D. (2017). Pediatric high-grade glioma: current molecular landscape and therapeutic approaches. Journal of Neuro-Oncology, 134(3), 541-549. doi:10.1007/s11060-017-2393-0

(8) Chamdine, O., & Gajjar, A. (2014). Molecular characteristics of pediatric high-grade gliomas. CNS Oncol, 3(6), 433-443. doi:10.2217/cns.14.43

(9) Behjati, S., Gilbertson, R. J., & Pfister, S. M. (2021). Maturation Block in Childhood Cancer. Cancer Discovery, 11(3), 542-544. doi:10.1158/2159-8290.Cd-20-0926

(10) Smith, H. L., Wadhwani, N., & Horbinski, C. (2022). Major Features of the 2021 WHO Classification of CNS Tumors. Neurotherapeutics. doi:10.1007/s13311-022-01249-0

(11) Metselaar, D. S. (2021a). Novel Therapeutic Strategies in Aggressive Pediatric Brain Tumours: Navigating the Epigenetic Landscape. (PhD thesis). Amsterdam University Medical Center, Amsterdam. (ISBN: 978-94-6421-560-1)

(12) Metselaar, D. S., du Chatinier, A., Stuiver, I., Kaspers, G. J. L., & Hulleman, E. (2021b). Radiosensitization in Pediatric High-Grade Glioma: Targets, Resistance and Developments. Frontiers in Oncology, 11. doi:10.3389/fonc.2021.662209

(13) Rizzo, D., Ruggiero, A., Martini, M., Rizzo, V., Maurizi, P., & Riccardi, R. (2015). Molecular Biology in Pediatric High-Grade Glioma: Impact on Prognosis and Treatment. Biomed Res Int, 2015, 215135. doi:10.1155/2015/215135

(14) Greuter, L., Guzman, R., & Soleman, J. (2021). Pediatric and Adult Low-Grade Gliomas: Where Do the Differences Lie? Children (Basel), 8(11).

doi:10.3390/children8111075

(15) Hauser, P. (2021). Classification and Treatment of Pediatric Gliomas in the Molecular Era. Children (Basel), 8(9). doi:10.3390/children8090739

(16) Di Ruscio, V., Carai, A., Del Baldo, G., Vinci, M., Cacchione, A., Miele, E., . . . Mastronuzzi, A. (2022). Molecular Landscape in Infant High-Grade Gliomas: A Single Center Experience. Diagnostics (Basel), 12(2). doi:10.3390/diagnostics12020372

(17) Rechberger, J. S., Nesvick, C. L., & Daniels, D. J. (2022). Atypical teratoid rhabdoid tumor (ATRT): disease mechanisms and potential drug targets. Expert Opinion on Therapeutic Targets, 26(3), 187-192. doi:10.1080/14728222.2022.2040017

(18) Nesvick, C. L., Lafay-Cousin, L., Raghunathan, A., Bouffet, E., Huang, A. A., & Daniels, D. J. (2020). Atypical teratoid rhabdoid tumor: molecular insights and translation to novel therapeutics. J Neurooncol, 150(1), 47-56. doi:10.1007/s11060-020-03639-w

(19) Cacciotti, C., Fleming, A., & Ramaswamy, V. (2020). Advances in the molecular classification of pediatric brain tumors: a guide to the galaxy. The Journal of Pathology, 251(3), 249-261. doi:https://doi.org/10.1002/path.5457

(20) Kadoch, C., Hargreaves, D. C., Hodges, C., Elias, L., Ho, L., Ranish, J., & Crabtree, G. R. (2013). Proteomic and bioinformatic analysis of mammalian SWI/SNF complexes identifies extensive roles in human malignancy. Nat Genet, 45(6), 592-601. doi:10.1038/ng.2628

(21) Erkek, S., Johann, P. D., Finetti, M. A., Drosos, Y., Chou, H. C., Zapatka, M., . . . Kool, M. (2019). Comprehensive Analysis of Chromatin States in Atypical Teratoid/Rhabdoid Tumor Identifies Diverging Roles for SWI/SNF and Polycomb in Gene Regulation. Cancer Cell, 35(1), 95-110.e118. doi:10.1016/j.ccell.2018.11.014

(22) Ho, B., Johann, P. D., Grabovska, Y., De Dieu Andrianteranagna, M. J., Yao, F., Frühwald, M., . . . Kool, M. (2020). Molecular subgrouping of atypical teratoid/rhabdoid tumors-a reinvestigation and current consensus. Neuro Oncol, 22(5), 613-624. doi:10.1093/neuonc/noz235

(23) Richardson, E. A., Ho, B., & Huang, A. (2018). Atypical Teratoid Rhabdoid Tumour : From Tumours to Therapies. J Korean Neurosurg Soc, 61(3), 302-311. doi:10.3340/jkns.2018.0061

(24) Himes, B. T., Zhang, L., & Daniels, D. J. (2019). Treatment Strategies in Diffuse Midline Gliomas With the H3K27M Mutation: The Role of Convection-Enhanced Delivery in Overcoming Anatomic Challenges. Frontiers in Oncology, 9. doi:10.3389/fonc.2019.00031

(25) Korshunov, A., Schrimpf, D., Ryzhova, M., Sturm, D., Chavez, L., Hovestadt, V., . . . Jones, D. T. W. (2017). H3-/IDH-wild type pediatric glioblastoma is comprised of molecularly and prognostically distinct subtypes with associated oncogenic drivers. Acta Neuropathologica, 134(3), 507-516. doi:10.1007/s00401-017-1710-1

(26) Aldape, K., Zadeh, G., Mansouri, S., Reifenberger, G., & von Deimling, A. (2015). Glioblastoma: pathology, molecular mechanisms and markers. Acta Neuropathol, 129(6), 829-848. doi:10.1007/s00401-015-1432-1

(27) Bernstock, J. D., Hoffman, S. E., Kappel, A. D., Valdes, P. A., Essayed, W., Klinger, N. V., . . . Friedman, G. K. (2022). Immunotherapy approaches for the treatment of diffuse midline gliomas. Oncoimmunology, 11(1), 2124058. doi:10.1080/2162402x.2022.2124058

(28) Lucas, C.-H. G., Mueller, S., Reddy, A., Taylor, J. W., Oberheim Bush, N. A., Clarke, J. L., . . . Solomon, D. A. (2021). Diffuse hemispheric glioma, H3 G34-mutant: Genomic landscape of a new tumor entity and prospects for targeted therapy. Neuro-Oncology, 23(11), 1974-1976. doi:10.1093/neuonc/noab184

(29) Hu, W., Duan, H., Zhong, S., Zeng, J., & Mou, Y. (2022). High frequency of PDGFRA and MUC family gene mutations in diffuse hemispheric glioma, H3 G34-mutant: a glimmer of hope? J Transl Med, 20(1), 64. doi:10.1186/s12967-022-03258-1

(30) Park, M., Han, J. W., Hahn, S. M., Lee, J. A., Kim, J. Y., Shin, S. H., . . . Lyu, C. J. (2021). Atypical Teratoid/Rhabdoid Tumor of the Central Nervous System in Children under the Age of 3 Years. Cancer Res Treat, 53(2), 378-388. doi:10.4143/crt.2020.756

(31) Batra, V., Sands, S. A., Holmes, E., Geyer, J. R., Yates, A., Becker, L., . . . Finlay, J. L. (2014). Long-term survival of children less than six years of age enrolled on the CCG-945 phase III trial for newly-diagnosed high-grade glioma: a report from the Children's Oncology Group. Pediatr Blood Cancer, 61(1), 151-157. doi:10.1002/pbc.24718

(32) Jones, C., Karajannis, M. A., Jones, D. T. W., Kieran, M. W., Monje, M., Baker, S. J., . . . Weiss, W. A. (2017). Pediatric high-grade glioma: biologically and clinically in need of new thinking. Neuro Oncol, 19(2), 153-161. doi:10.1093/neuonc/now101

(33) Bhowmik, A., Khan, R., & Ghosh, M. K. (2015). Blood brain barrier: a challenge for effectual therapy of brain tumors. Biomed Res Int, 2015, 320941. doi:10.1155/2015/320941

(34) Jahangiri, A., Chin, A. T., Flanigan, P. M., Chen, R., Bankiewicz, K., & Aghi, M. K. (2017). Convection-enhanced delivery in glioblastoma: a review of preclinical and clinical studies. Journal of Neurosurgery JNS, 126(1), 191-200. doi:10.3171/2016.1.Jns151591

(35) Arvanitis, C. D., Ferraro, G. B., & Jain, R. K. (2020). The blood–brain barrier and blood–tumour barrier in brain tumours and metastases. Nature Reviews Cancer, 20(1), 26-41. doi:10.1038/s41568-019-0205-x

(36) Meng, Y., Pople, C. B., Budiansky, D., Li, D., Suppiah, S., Lim-Fat, M. J., . . . Lipsman, N. (2022). Current state of therapeutic focused ultrasound applications in neuro-oncology. Journal of Neuro-Oncology, 156(1), 49-59. doi:10.1007/s11060-021-03861-0

(37) Englander, Z. K., Wei, H.-J., Pouliopoulos, A. N., Bendau, E., Upadhyayula, P., Jan, C.-I., . . . Wu, C.-C. (2021). Focused ultrasound mediated blood–brain barrier opening is

safe and feasible in a murine pontine glioma model. Scientific Reports, 11(1), 6521. doi:10.1038/s41598-021-85180-y

(38) Dubois, L. G., Campanati, L., Righy, C., D'Andrea-Meira, I., Spohr, T. C., Porto-Carreiro, I., . . . Moura-Neto, V. (2014). Gliomas and the vascular fragility of the blood brain barrier. Front Cell Neurosci, 8, 418. doi:10.3389/fncel.2014.00418

(39) Upton, D. H., Ung, C., George, S. M., Tsoli, M., Kavallaris, M., & Ziegler, D. S. (2022). Challenges and opportunities to penetrate the blood-brain barrier for brain cancer therapy. Theranostics, 12(10), 4734-4752. doi:10.7150/thno.69682

(40) Mathew, E. N., Berry, B. C., Yang, H. W., Carroll, R. S., & Johnson, M. D. (2022). Delivering Therapeutics to Glioblastoma: Overcoming Biological Constraints. Int J Mol Sci, 23(3). doi:10.3390/ijms23031711

(41) Dong, X. (2018). Current Strategies for Brain Drug Delivery. Theranostics, 8(6), 1481-1493. doi:10.7150/thno.21254

(42) Claes, A., Idema, A. J., & Wesseling, P. (2007). Diffuse glioma growth: a guerilla war. Acta Neuropathol, 114(5), 443-458. doi:10.1007/s00401-007-0293-7

(43) Tosi, U., & Souweidane, M. (2020). Convection Enhanced Delivery for Diffuse Intrinsic Pontine Glioma: Review of a Single Institution Experience. Pharmaceutics, 12(7). doi:10.3390/pharmaceutics12070660

(44) Pilkington, G. J. (1994). Tumour Cell Migration in the Central Nervous System. Brain Pathology, 4(2), 157-166. doi:https://doi.org/10.1111/j.1750-3639.1994.tb00826.x

(45) Hill, S. M., Padilla-Rodriguez, M., Clements, A., Sweetland, J. A., Parker, S. S., Warfel, N. A., & Mouneimne, G. (2022). Optimized in vitro three-dimensional invasion assay for quantifying a wide range of cancer cell invasive behavior. STAR Protocols, 3(3), 101516. doi:https://doi.org/10.1016/j.xpro.2022.101516

(46) Manini, I., Caponnetto, F., Bartolini, A., Ius, T., Mariuzzi, L., Di Loreto, C., . . . Cesselli, D. (2018). Role of Microenvironment in Glioma Invasion: What We Learned from In Vitro Models. Int J Mol Sci, 19(1). doi:10.3390/ijms19010147

(47) Berens, E. B., Holy, J. M., Riegel, A. T., & Wellstein, A. (2015). A Cancer Cell Spheroid Assay to Assess Invasion in a 3D Setting. J Vis Exp(105). doi:10.3791/53409

(48) Pibuel, M. A., Poodts, D., Díaz, M., Hajos, S. E., & Lompardía, S. L. (2021). The scrambled story between hyaluronan and glioblastoma. Journal of Biological Chemistry, 296, 100549. doi:https://doi.org/10.1016/j.jbc.2021.100549

(49) Beliën, A. T., Paganetti, P. A., & Schwab, M. E. (1999). Membrane-type 1 matrix metalloprotease (MT1-MMP) enables invasive migration of glioma cells in central nervous system white matter. J Cell Biol, 144(2), 373-384. doi:10.1083/jcb.144.2.373

(50) Beadle, C., Assanah, M. C., Monzo, P., Vallee, R., Rosenfeld, S. S., & Canoll, P. (2008). The role of myosin II in glioma invasion of the brain. Mol Biol Cell, 19(8), 3357-

3368. doi:10.1091/mbc.e08-03-0319

(51) Brekhman, V., & Neufeld, G. (2009). A novel asymmetric 3D in-vitro assay for the study of tumor cell invasion. BMC Cancer, 9, 415. doi:10.1186/1471-2407-9-415

(52) Aisenbrey, E. A., & Murphy, W. L. (2020). Synthetic alternatives to Matrigel. Nat Rev Mater, 5(7), 539-551. doi:10.1038/s41578-020-0199-8

(53) Menyhárt, O., Harami-Papp, H., Sukumar, S., Schäfer, R., Magnani, L., de Barrios, O., & Győrffy, B. (2016). Guidelines for the selection of functional assays to evaluate the hallmarks of cancer. Biochimica et Biophysica Acta (BBA) - Reviews on Cancer, 1866(2), 300-319. doi:https://doi.org/10.1016/j.bbcan.2016.10.002

(54) Ran, F. A., Hsu, P. D., Wright, J., Agarwala, V., Scott, D. A., & Zhang, F. (2013). Genome engineering using the CRISPR-Cas9 system. Nature Protocols, 8(11), 2281-2308. doi:10.1038/nprot.2013.143

(55) Asmamaw, M., & Zawdie, B. (2021). Mechanism and Applications of CRISPR/Cas-9-Mediated Genome Editing. Biologics, 15, 353-361. doi:10.2147/btt.S326422

(56) Joung, J., Konermann, S., Gootenberg, J. S., Abudayyeh, O. O., Platt, R. J., Brigham, M. D., . . . Zhang, F. (2017). Genome-scale CRISPR-Cas9 knockout and transcriptional activation screening. Nature Protocols, 12(4), 828-863. doi:10.1038/nprot.2017.016

(57) Bock, C., Datlinger, P., Chardon, F., Coelho, M. A., Dong, M. B., Lawson, K. A., . . . Zhuang, X. (2022). High-content CRISPR screening. Nature Reviews Methods Primers, 2(1), 8. doi:10.1038/s43586-021-00093-4

(58) Park, S. B., Uchida, T., Tilson, S., Hu, Z., Ma, C. D., Leek, M., . . . Liang, T. J. (2022). A dual conditional CRISPR-Cas9 system to activate gene editing and reduce off-target effects in human stem cells. Molecular Therapy - Nucleic Acids, 28, 656-669. doi:https://doi.org/10.1016/j.omtn.2022.04.013

(59) Yu, J. S. L., & Yusa, K. (2019). Genome-wide CRISPR-Cas9 screening in mammalian cells. Methods, 164-165, 29-35. doi:https://doi.org/10.1016/j.ymeth.2019.04.015

(60) Prolo, L. M., Li, A., Owen, S. F., Parker, J. J., Foshay, K., Nitta, R. T., . . . Grant, G. A. (2019). Targeted genomic CRISPR-Cas9 screen identifies MAP4K4 as essential for glioblastoma invasion. Scientific Reports, 9(1), 14020. doi:10.1038/s41598-019-50160-w

(61) Armento, A., Ehlers, J., Schötterl, S., & Naumann, U. (2017). Molecular Mechanisms of Glioma Cell Motility. In S. D. Vleeschouwer (Ed.), Glioblastoma.

(62) Meel, M. H., Metselaar, D. S., Waranecki, P., Kaspers, G. J. L., & Hulleman, E. (2018). An efficient method for the transduction of primary pediatric glioma neurospheres. MethodsX, 5, 173-183. doi:10.1016/j.mex.2018.02.006

(63) Metselaar, D. S., du Chatinier, A., Meel, M. H., Ter Huizen, G., Waranecki, P., Goulding, J. R., . . . Hulleman, E. (2022). AURKA and PLK1 inhibition selectively and

synergistically block cell cycle progression in diffuse midline glioma. iScience, 25(6), 104398-104398. doi:10.1016/j.isci.2022.104398

(64) Meel, M. H., de Gooijer, M. C., Metselaar, D. S., Sewing, A. C. P., Zwaan, K., Waranecki, P., . . . Hulleman, E. (2020b). Combined Therapy of AXL and HDAC Inhibition Reverses Mesenchymal Transition in Diffuse Intrinsic Pontine Glioma. Clin Cancer Res, 26(13), 3319-3332. doi:10.1158/1078-0432.Ccr-19-3538

(65) Da Silva, L., Bray, J. K., Bulut, G., Jiang, J., & Schmittgen, T. D. (2020). Method for improved integrity of RNA isolated from Matrigel cultures. MethodsX, 7, 100966. doi:10.1016/j.mex.2020.100966

(66) Li, W., Köster, J., Xu, H., Chen, C.-H., Xiao, T., Liu, J. S., . . . Liu, X. S. (2015). Quality control, modeling, and visualization of CRISPR screens with MAGeCK-VISPR. Genome Biology, 16(1), 281. doi:10.1186/s13059-015-0843-6

(67) Ma, H., Dang, Y., Wu, Y., Jia, G., Anaya, E., Zhang, J., . . . Wu, H. (2015). A CRISPR-Based Screen Identifies Genes Essential for West-Nile-Virus-Induced Cell Death. Cell Rep, 12(4), 673-683. doi:10.1016/j.celrep.2015.06.049

(68) Belykh, E., Shaffer, K. V., Lin, C., Byvaltsev, V. A., Preul, M. C., & Chen, L. (2020). Blood-Brain Barrier, Blood-Brain Tumor Barrier, and Fluorescence-Guided Neurosurgical Oncology: Delivering Optical Labels to Brain Tumors. Frontiers in Oncology, 10. doi:10.3389/fonc.2020.00739

(69) Cockle, J. V., Picton, S., Levesley, J., Ilett, E., Carcaboso, A. M., Short, S., . . . Brüning-Richardson, A. (2015). Cell migration in paediatric glioma; characterisation and potential therapeutic targeting. Br J Cancer, 112(4), 693-703. doi:10.1038/bjc.2015.16

(70) Park, J. B., Kwak, H. J., & Lee, S. H. (2008). Role of hyaluronan in glioma invasion. Cell Adh Migr, 2(3), 202-207. doi:10.4161/cam.2.3.6320

(71) Thomas, I. Z., & Aleksander, S. (2018). HyStem®: A Unique Clinical Grade Hydrogel for Present and Future Medical Applications. In P. Lăcrămioara, G. Mihaela Violeta, & D.-P. Cristina-Elena (Eds.), Hydrogels (pp. Ch. 5). Rijeka: IntechOpen.

(72) Lan, T., Pang, J., Wu, Y., Zhu, M., Yao, X., Wu, M., . . . Chen, Y. (2016). Cross-linked hyaluronic acid gel inhibits metastasis and growth of gastric and hepatic cancer cells: in vitro and in vivo studies. Oncotarget, 7(40), 65418-65428. doi:10.18632/oncotarget.11739

(73) Yang, C., Cao, M., Liu, H., He, Y., Xu, J., Du, Y., . . . Gao, F. (2012). The high and low molecular weight forms of hyaluronan have distinct effects on CD44 clustering. J Biol Chem, 287(51), 43094-43107. doi:10.1074/jbc.M112.349209

(74) Tan, J.-X., Wang, X.-Y., Li, H.-Y., Su, X.-L., Wang, L., Ran, L., . . . Ren, G.-S. (2011). HYAL1 overexpression is correlated with the malignant behavior of human breast cancer. International Journal of Cancer, 128(6), 1303-1315. doi:https://doi.org/10.1002/ijc.25460

(75) Tian, X., Azpurua, J., Hine, C., Vaidya, A., Myakishev-Rempel, M., Ablaeva, J., . . . Seluanov, A. (2013). High-molecular-mass hyaluronan mediates the cancer resistance of the naked mole rat. Nature, 499(7458), 346-349. doi:10.1038/nature12234

(76) Zanotelli, M. R., Rahman-Zaman, A., VanderBurgh, J. A., Taufalele, P. V., Jain, A., Erickson, D., . . . Reinhart-King, C. A. (2019). Energetic costs regulated by cell mechanics and confinement are predictive of migration path during decision-making. Nature Communications, 10(1), 4185. doi:10.1038/s41467-019-12155-z

(77) de Almeida, M., Hinterndorfer, M., Brunner, H., Grishkovskaya, I., Singh, K., Schleiffer, A., . . . Zuber, J. (2021). AKIRIN2 controls the nuclear import of proteasomes in vertebrates. Nature, 599(7885), 491-496. doi:10.1038/s41586-021-04035-8

(78) Wang, S., Wang, Y., Xiong, J., Bao, W., Li, Y., Qin, J., . . . Dong, Z. (2022). Novel Brain-Stiffness-Mimicking Matrix Gel Enables Comprehensive Invasion Analysis of 3D Cultured GBM Cells. Frontiers in Molecular Biosciences, 9. doi:10.3389/fmolb.2022.885806

(79) Tamai, S., Ichinose, T., Tsutsui, T., Tanaka, S., Garaeva, F., Sabit, H., & Nakada, M. (2022). Tumor Microenvironment in Glioma Invasion. Brain Sci, 12(4). doi:10.3390/brainsci12040505

(80) Lin, G. L., & Monje, M. (2017). A Protocol for Rapid Post-mortem Cell Culture of Diffuse Intrinsic Pontine Glioma (DIPG). J Vis Exp(121). doi:10.3791/55360

(81) Dull, T., Zufferey, R., Kelly, M., Mandel, R. J., Nguyen, M., Trono, D., & Naldini, L. (1998). A third-generation lentivirus vector with a conditional packaging system. J Virol, 72(11), 8463-8471. doi:10.1128/jvi.72.11.8463-8471.1998

(82) Wang, T., Wei, J. J., Sabatini, D. M., & Lander, E. S. (2014). Genetic Screens in Human Cells Using the CRISPR-Cas9 System. Science, 343(6166), 80-84. doi:doi:10.1126/science.1246981

Materials and Methods

Cell Lines

HSJD-DIPG-07 (H3.3 K27 altered), JHH-DIPG-01 (H3.3 K27 altered), VUMC-DIPG-08 (H3.3 K27 altered), VUMC-DIPG-F, VUMC-ATRT-01 (SHH), VUMC-ATRT-03 (SHH), CHLA-05-ATRT (SHH), CHLA-06-ATRT (MYC), OPBG-GBM-01 (H3-G34R/V), OPBG-DIPG-02 (H3.3 K27 altered), OPBG-DIPG-10 (H3.3 K27M), as well as murine cell lines IUE-24D3 (H3 WT), IUE-24B-7 (H3.3 K27M), IUE-26C-2 (H3.1 K27M), were all cultured in a Tumour Stem Media (TSM).[80] The TSM is composed of 250 mL Neurobasal-A medium (ThermoFisher Scientific, Waltham, MA, USA, #10888022), 250 mL DMEM/F12, HEPES (ThermoFisher Scientific, #31330095), 5 mL HEPES 1M (ThermoFisher Scientific, #15630056), 5 mL MEM non-essential amino acid solution 100x (ThermoFisher Scientific, #11140050), 5 mL GlutaMAX supplement 100x (ThermoFisher Scientific, #35050038), 5 mL Sodium Pyruvate 100mM (ThermoFisher Scientific, #11360070), 1 mL Primocin (InvioGen, San Diego, CA, USA, #ant-pm-2), and freshly supplemented with 50x B27 (without vitamin A) (ThermoFisher Scientific, #12587010), 20 ng/mL FGF-basic (Peprotech, Waltham, MA, USA, #AF-100-18B-1MG), 20ng/mL EGF (Peprotech, #AF-100-15-1MG), 10 ng/mL PDGF-AA (Peprotech, #100-13A-250uG), 10 ng/mL PDGF-BB (Peprotech, #100-14B-250uG), 5 µg/mL Heparin (Prinses Maxima Centrum Pharmacy) and 100x N-2 supplement (ThermoFisher Scientific, #17502048). The cells were cultured at 37°C and 5% CO_2.

Invasion Assay

Preparation of HyStem®-HP matrix

For the invasion assay, the HyStem®-HP (Advanced Biomatrix, Carlsbad, CA, USA, #GS315) was used as the major component of the assay. The gel was prepared following the standard protocol as provided by the manufacturer. The components of the HyStem®-HP (Advanced Biomatrix, #GS315) were brought to room temperature for 1 hour. Following this, 1 mL of degassed water was added to the Heprasil® and the Gelin-S®, and 0.5 mL of degassed water was added to the Extralink® using a 23G needle (Merkala, Alkmaar, Netherlands) and syringe. The vials were vortexed after the addition of water, and every 15 minutes thereafter for an hour. In-between vortexing the vials were placed horizontally on a shaker. Once the components were fully dissolved, the Heprasil® and Gelin-S® were combined into a single vial and the following growth factors were added to the mixture: 20 ng/mL FGF-basic (Peprotech, #AF-100-18B-1MG), 20ng/mL EGF (Peprotech, #AF-100-15-1MG), 10 ng/mL PDGF-AA (Peprotech, #100-13A-250uG), 10 ng/mL PDGF-BB (Peprotech, #100-14B-250uG). The HyStem®-HP was diluted 1:1 with TSM.

Drop Invasion Assay Preparation

Two 60 µL drops of HyStem®-HP (Advanced Biomatrix, #GS315) were pipetted 1 mm apart onto a 22 mm circular glass coverslip (Electron Microscope Sciences, Hatfield, PA, USA, #72224-01) in a 6-well plate (TPP, Trasadingen, Switzerland, #92006) and left to solidify for 90 minutes at 37°C and 5% CO_2. 4 µL of HyStem®-HP (Advanced Biomatrix, #GS315) containing 10,000 IUE-24B7 cells were pipetted in between the two circular drops of gel, creating a ‘bridge’ between the circles. The gel was left to solidify for 90 minutes at 37°C and

5% CO_2. 3 mL of TSM was added and the assay was left to incubate at 37°C and 5% CO_2 for 12 days. The plates were imaged using the Leica THUNDER Imager (Leica Microsystems) on day 0, day 4, day 8 and day 12. The images were processed using the Leica LAS X Life Science software. The invasion distance was determined by outlining the two drops and measuring the 20 random straight-line distances the cells invaded using ImageJ.

Dissolving HyStem®-HP matrix using Hyaluronidase

The HyStem®-HP (Advanced Biomatrix, #GS315) was cut-up using a scalpel and placed into a 15 mL tube. 400U of hyaluronidase enzyme () was added to the gel and by pipetting up and down every 15 minutes the gel was dissolved. The integrity of the cells was visualised using the Leica DMi1 (Leica Microsystems) and the Leica LAS X Life Sciences software.

Lentivirus Production

The lentiviral transfection procedure was necessary to establish several different cell lines carrying different plasmids of Cas9 or the CRISPR-KO library. HEK293T cells were cultured in DMEM (ThermoFisher Scientific, #21885025) + 10% heat-inactivated foetal bovine serum (FBS) + 1% Penicillin-Streptomycin (Merck-Sigma Aldrich, Darmstadt, Germany, #P0781-100ML) and used to assemble lentiviruses following the standard polyethyleneimine (PEI) protocol. The transfection solution contained 3 ug pMD2.G gifted from Didier Trono (Addgene plasmid # 12259; http://n2t.net/addgene:12259; RRID: Addgene_12259), 5ug pMDLg/pRRE gifted from Didier Trono (Addgene plasmid # 12251; http://n2t.net/addgene:12251; RRID: Addgene_12251), 2.5 ug pRSV-REV gifted from Didier Trono (Addgene plasmid #12253; http://n2t.net/addgene:12253; RRID: Addgene_12253), and 5 ug of the desired vector **(Table 3) (Appendix 3)**. These 3rd generation lentiviral packaging plasmids are described by Dull et al. (1998).[81] After 24 hours, the medium containing the transfection agents was removed and replaced with TSM + 10% heat inactivated FBS. After 48 hours, the medium was removed from the HEK293T cells and stored at 4 °C. The HEK293T cells were then refreshed with TSM + 10% heat-inactivated FBS. After 72 hours, the medium was removed from the HEK293T cells and pooled with the medium from previous days. The pooled virus-containing media was filtered using a sterile 0.45µm filter to remove any remaining HEK293T cells and was used freshly or stored at -80 °C.

Table 3: Vectors used for HEK293T transfection

Plasmid	Plasmid size (bp)	5' Sequencing Primer	Gifted From
pCW-Cas9 Puro	11,885	AGCTCGTTTAGTG AACCGTCAGATC	Eric Lander & David Sabatini (Addgene plasmid # 50661 ; http://n2t.net/addgene:50661 ; RRID:Addgene_50661)
pCW-Cas9 Blast	11,687	Unknown	Mohan Babu (Addgene plasmid # 83481 ; http://n2t.net/addgene:83481 ; RRID:Addgene_83481)
pCW-Cas9-	12,674	AGCTCGTTTAGTG AACCGTCAGATC	Ronald Germain (Addgene plasmid # 167928 ;

2A-EGFP			http://n2t.net/addgene:167928 ; RRID:Addgene_167928)
pHIV-EGFP	7,686	TGGAATTTGCCCTTTTTGAG	Bryan Welm & Zena Werb (Addgene plasmid # 21373 ; http://n2t.net/addgene:21373 ; RRID:Addgene_21373)
Library	**Guide RNAs**	**Genes Targeted**	**Gifted From**
Human lentiviral CRISPR library v1	77,406	20,121	Kosuke Yusa (Addgene #67989)

Lentivirus Transduction

The methods described by Meel *et al.* (2018) was used to transduce primary glioma neurospheres. The neurospheres were dissociated and made single-celled with Accutase (Merck-Sigma Aldrich, #A6964-100ML) and a 70 µm EASYstrainer (Greiner Bio-One, Alphen aan den Rijn, Netherlands, #542070). The glioma cells were seeded in 6 well-plates at a density of 3×10^5 cells in 1.5 mL TSM without FBS. The glioma cells were then left to form neurospheres for 24 hours at 37°C and 5% CO_2. After 24 hours, the Cas9/CRISPR-KO lentivirus in TSM supplemented with 10% heat-inactivated FBS was added to the glioma cells at a 1:1 ratio. The glioma neuroshperes are temporarily exposed to FBS because a cell adherent state was shown to increase transduction efficiency.[62] The neurospheres were incubated for 24 hours at 37°C and 5% CO_2 to allow for partial attachment of glioma cells. Following partial attachment, the media was replaced with TSM without FBS. The glioma neuroshperes were then left to recover from the transduction procedure for a period of 7 days. The media was replaced as often as necessary, and trypsin (Merck-Sigma Aldrich, #T3924) was used to accelerate the detachment of the neurospheres. The transduced cells were then selected using appropriate concentrations of puromycin (Sigma-Aldrich, Saint Louis, MO, USA, #P8833) or blasticidin (Sigma-Aldrich, #203350), if necessary, for 7 days. The incubation period of neurospheres after the addition of virus was reduced for certain cell lines that were more sensitive to FBS.

Selection Procedure

The selection procedure for each cell line differed slightly based on resistance and the plasmid used for transduction. The selection procedure for each plasmid transduced into the pHGG and ATRT cell lines is summarised in **Table 4** and plasmid maps can be found in **Appendix 3**. Some cell lines, such as the IUE-murine cells, required higher concentrations of selection agents due to greater resistance. The selection procedure was performed for a minimum of 1 week and at least until all the control groups we not viable.

Table 4: Summary of selection procedure used for cells transduced with specific plasmids/libraries.

Plasmid/ Library	Selection procedure	Concentration
pCW-Cas9 puromycin	Puromycin	2 µg/mL
pCW-Cas9 blasticidin	Blasticidin	15 µg/mL
pCW-Cas9-2A-EGFP	FACS (GFP)	NA
Human CRISPR kinase-enriched pool library	Blasticidin	15 µg/mL
Human CRISPR nucleosome-enriched pool library	Blasticidin	15 µg/mL
Mouse kinome CRISPR pooled library (Brie)	Puromycin	2 µg/mL
Human lentiviral CRISPR library v1	FACS (GFP)	NA

FACS

Cells were collected by centrifuging at 250 rpm for 5 minutes. The medium was discarded, and the cell pellet was resuspended in 2 mL Accutase® solution (Sigma-Aldrich, #A6964) and incubated in a water bath at 37°C for 4 minutes. 5 mL of TSM was added to the Accutase-cell mixture and the cells were collected by centrifuging 250 rpm for 5 minutes. The cell pellet was resuspended in 500 µL PBS (ThermoFisher Scientific, #14190-169) and pipetted through a 70 µm EASYstrainer (Greiner Bio-One, #542070). The cell suspension was then filtered through 5 mL falcon tubes (Corning, Somerville, MA, USA, #352235) and stored on ice until time of sorting. A Sony SH800S cell sorter (Sony Corporation, Tokyo, Japan) was used with 100 µm sorting chip (Sony, #LE-C3210), 488nm beam, and 561nm beam. The cells were analysed using the Sony cell sorter software (Sony Corporation) and GFP positive cells were collected.

Western Blotting

Transduced cells were harvested under optimal growth conditions or after 24-hour exposure to 0.5 µg/mL or 1.0 µg/mL of doxycycline, washed with ice-cold PBS (ThermoFisher Scientific, #14190-169) and snap frozen in liquid nitrogen. A lysis buffer was prepared using x20 β-glycerol phosphate, x100 dithiothreitol (DTT), x1000 Na30V, x10 protease inhibitor cocktail (PIC), x500 leupeptin, x500 pepstatin A, and x500 aprotinin, diluted in a radioimmunoprecipitation assay (RIPA) buffer. An appropriate volume of the lysis buffer was added to each sample, which was left on ice for 1 hour and vortexed every 15 minutes. The samples were spun down for 15 minutes at 14,000g and 4°C, after which the pellet was discarded. The protein concentrations of each sample were then measured by creating a standard curve using different concentrations of the Bio-rad protein assay standard II (Bio-Rad Laboratories, Hercules, CA, USA, #5000007). The samples were prepared for protein concentration measurements by performing appropriate dilutions and adding the Bio-rad staining protein assay solution (Bio-Rad Laboratories, #5000006) to each sample. The concentration of each sample was determined using the SpectraMax iD3 Multi-Mode Microplate Reader (Molecular Devices) with an absorbance setting of 595nm. Following the determination of sample concentrations, NuPAGE LDS sample buffer NP-007 (4x) (ThermoFisher Scientific, #NP0007) was added to 50 µg of each sample and was placed on a heatblock for 5 minutes at 95°C. The 456-1094 Bio-rad precast gels (Bio-Rad, #4561094) were used in a 1x TGS running buffer. 20 µL of each sample was loaded onto the gel together with 5 µL of ladder PageRuler Plus Prestige (ThermoFisher Scientific, #26619). The gel was run at 100V for 2 hours. The gel was transferred to a Bio-rad membrane (Bio-rad #1704158) using the trans-Blot® Turbo Transfer System (Bio-Rad). The membrane was blocked for 30 minutes using 5mL blocking buffer (Rockland Immunochemicals, Pottstown, PA, USA, #MB-070) in

a rotating 50mL tube at room temperature (RT). Then using a 50:50 solution of blocking buffer (Rockland Immunochemicals, #MB-070) and 1x TBST, the primary monoclonal ANTI-FLAG® M2 antibody produced in mouse (x1000) (Sigma-Aldrich, #F3165) was added to the membrane and left to incubate overnight at 4°C whilst rotating. The membrane was washed three times for 15 minutes in 1x TBST. An IRDye® 800CW goat anti-mouse IgG secondary antibody (x10000) (Li-Cor Biosciences, Lincoln, NE, USA, #926-32210) was then used to stain the membrane in a 50:50 blocking buffer and x1 TBST solution for 1 hour at RT. The membrane was washed three times for 15 minutes in 1x TBST. Imaging was then performed using the Odyssey® CLx Infared Imaging Systems (Li-Cor Biosciences). The same 2-step antibody staining procedure was then performed for actin staining using an anti-actin antibody, clone c4 (Sigma-Aldrich, #MAB1501) as the primary antibody, which was incubated for 1 hour at RT in a rotating 50 mL tube. The IRDye® 680RD goat anti-mouse IgG secondary antibody (Li-Cor, #926-68070) was then used for actin staining.

Library Preparation and Sequencing

The C3040I high efficiency transformation protocol provided by New England BioLabs Inc. was used to perform the transformation of NEB® Stable Competent *E.coli* with 4 different CRISPR libraries: Human CRISPR enriched pool library gifted from David Sabatini and Eric Lander (Addgene #51044 and #51047), the Mouse Kinome CRISPR pooled library (Brie) gifted from John Doench and David Root (Addgene #75316), and the Human lentiviral CRISPR library v1 gifted from Haoquan Wu (Addgene #69763) **(Appendix 3)**. Each transformed library was plated on LB agar plates containing ampicillin at x10, x100 and x1000 dilutions. Three liquid cultures were prepared using in 500 mL Erlenmeyer flasks containing lysogeny broth (LB), x200 TB salts, x1000 carbenicillin and a respective transformed CRISPR library. The TB salt solution contained 0.2M potassium phosphate, monobasic (Sigma-Aldrich, #7778-77-0) and 0.7M potassium phosphate dibasic (Sigma-Aldrich, #7758-11-4). The LB cultures were left to expand overnight at 37°C and 250 rpm. Using known information on the growth rate of NEB® Stable Competent *E.coli* and the number of colonies formed on the overnight plates at different concentrations, an appropriate dilution was used to further expand the libraries in a total of 1.2 litres of LB, x200 TB salts and x1000 carbenicillin for each CRISPR library. This was left to expand overnight at 37°C and 250 rpm. Following library expansion, the bacterial cultures were centrifuged at max speed for 15 minutes to collect the bacterial pellets containing the CRISPR libraries. A NucleoBond Xtra Maxi kit for transfection-grade plasmid DNA (Macherey-Nagel, Duren, Germany, #740414.50) was used to extract the fresh transformant plasmids from the *E.coli.,* after which the concentration of extracted plasmids was measured using the NanoDrop™ One (ThermoFisher Scientific). To determine the size of the plasmids and therefore quality, high-fidelity Not1 restriction enzyme (New England Biolabs, Inc., Ipscich, MA, USA, #R0189S) was used to perform a single cut on the plasmids. A standard gel electrophoresis was performed, and the quality of the extracted plasmids was assessed.

Once the quality of the extracted plasmids was satisfactory, the libraries were prepared for Ilumina sequencing for further quality control and analysis. The quality checks for each library samples were performed in-house. The PCR protocol for Ilumina Sequencing was adapted from

Wang *et al.* (2014).[82] The following reaction mixture for each library was aliquoted in 50 µL into 0.2 mL PCR tubes (Greiner Bio-One, #671201): 1.5 µg genomic DNA, 6 µL forwards sgRNA PCR primer (10µM), 6 µL sample-specific barcoded reverse sgRNA PCR primer (10µM), 75 µL PCR Master Mix, and 60 µL ultra-pure water. The reactions were then amplified in a T100 thermal cycler (Bio-Rad, #1861096) with the following programme:

1 cycle	98°C	2 minutes
22 cycles		98°C 10 seconds
		60°C 15 seconds
		72°C 45 seconds
1 cycle	72°C	5 minutes
1 cycle	4°C	HOLD

The PCR products were loaded on a 1% agarose gel with 1% TAE buffer for 90 minutes at 120V. The plasmids were extracted using the Thermo Scientific GeneJET gel extraction kit (Thermo Scientific, #K0691) and the quality of the extracted plasmids was assessed on the 2100 Bioanalyzer (Agilent Technologies, Amstelveen, Netherlands). The samples were sent to GenomeScan (Leiden University Medical Center) for Illumina sequencing.

RNA Sequencing and Analysis

To determine the integrity of the CRISPR libraries and to obtain sgRNA counts, the MAGeCK VISPR (model-based analysis of genome-wide CRSIPR-Cas9 Knockout) pipeline was implemented. Galaxy Europe (usegalaxy.eu), an open, web-based data analysis environment was used to obtain read quality reports and collect sgRNA read counts from the different library sample reads. The functions ‘FastQC’ and ‘MAGeCK count’ were used to determine the integrity of the sequenced libraries.

Appendices

Appendix 1: Additional methods used for the optimisation of the invasion assay

Appendix 1A: Testing the suitability of HyStem®-HP

To determine if the HyStem®-HP (Advanced Biomatrix, #GS315) is a suitable matrix for the invasion assays, 10,000 HSJD-DIPG-07 cells, 10,000 VUMC-DIPG-F cells and 10,000 IUE-24B7 cells were made single cell using Accutase (Merck-Sigma Aldrich, #542070) and a 70 µm EASYstrainer (Greiner Bio-One, #542070), and seeded into a U-bottom 96-well well plate (Greiner Bio-One, #650970) with 100 µL TSM, and incubated overnight at 37°C and 5% CO_2 for spheroid formation. 80 µL of TSM was removed from each well containing spheroids and either 80 µL HSHP gel (Advanced Biomatrix, #GS315), 80 µL Matrigel (Corning, #354248) or 80 µL of TSM was carefully added on top of the spheroids. The U-bottom 96 well plate (Greiner Bio-One, #650970) was centrifuged at 250g for 5 mins to ensure the spheroids remained in the centre of the wells prior to gel solidification and were left to incubate for 1 hour at 37°C and 5% CO_2. 50 µL of TSM was later added to each well and the spheroids in gel were incubated for 6 days at 37°C and 5% CO_2. The Leica Dmi8 S Platform Live cell microscope (Leica Microsystems, Wetzlar, Germany) was used to image the spheroids at day 0, day 2 and day 6. Relative invasion was measured using ImageJ and is defined as the area of the invasion zone compared to the area of the central spheroid.

Appendix 1B: Invasion assay set-up to distinguish migrating cells from non-migrating cells using BacMam 2.0 technology and a three-layer matrix

To establish if the CellLight™ Tubulin-GFP, BacMam 2.0 (ThermoFisher Scientific, #C10509) was a suitable method to distinguish migrating cells from non-migrating cells, an invasion assay was performed in a flat-bottom 96 well plate (Greiner Bio-One, #655180) containing three distinct layers of HyStem®-HP (Advanced Biomatrix, #GS315) matrix: an empty gel layer, a gel layer containing CellLight™ Tubulin-GFP, BacMam 2.0 (ThermoFisher Scientific, #C10509), and a gel layer containing 10,000 HSJD-DIPG-07 cells. The lid of the flat-bottom 96 well plate (Greiner Bio-One, #655180) was replaced with a plate adhesive (Bio-Rad, #MSB1001) that was punctured using a 26G needle (Merkala). 98 µL of empty gel was injected into a flat-bottom 96-well well (Greiner Bio-One, #655180) and kept at a 90°-degree angle for 90 minutes at RT. Next, 98 µL of gel containing 3 µL of BacMam 2.0 (ThermoFisher Scientific, #C10509) was injected above the solidified layer of empty gel in the flat-bottom 96-well well (Greiner Bio-One, #655180) and kept at a 90°-degree angle for 90 minutes at RT. The final 196 µL of gel containing 10,000 HSJD-DIPG-07 cells was injected above the solidified layers of gel in the flat-bottom 96-well well (Greiner Bio-One, #655180) and kept at a 90°-degree angle for 90 minutes at RT. 50 µL of TSM was added ontop of the gel, and the invasion assay was left to incubate for 4 days at 37°C and 5% CO_2. At day 4, X Hoechst 33342 solution (ThermoFisher Scientific, #62249) was used to visualise cells. The invasion of cells was monitored using the Leica Dmi8 S Platform Live cell microscope (Leica Microsystems, Wetzlar, Germany) on Day 0 and Day 4.

Appendix 1C: The angiogenesis slide, 8-well slide, and gel slice hypothesis for developing a high throughput invasion assay using BacMam 2.0

A µ-Slide 8 well (Ibidi, Grafelfing, Germany, #80826) chambered slide, a µ-Slide angiogenesis (Ibidi, #81506) slide, and cells seeded into a slice made in a gel were hypothesised to result in better visualisation outcomes for the invasion assay.

Chambered slide hypothesis

The invasion assay was performed in a µ-Slide 8 well (Ibidi, #80826) chambered slide containing two layers of HyStem®-HP (Advanced Biomatrix, #GS315) matrix: a layer with 3 µL of BacMam 2.0 (ThermoFisher Scientific, #C10509) and 1 µL Goat Anti-Mouse IgG H&L (Alexa Fluor® 568) (Abcam, Cambridge, United Kingdom, #ab175473), and a layer with 10,000 HSJD-DIPG-07 cells. It was hypothesised that the secondary antibody would remain fixed in its assigned layer of gel, distinguishing one layer from the other layer. Firstly, the lid of the µ-Slide 8 well (Ibidi, #80826) was replaced with a plate adhesive (Bio-Rad, #MSB1001) that was punctured using a 26G needle (Merkala). 150 µL of gel containing the BacMam 2.0 (ThermoFisher Scientific, #C10509) and Goat Anti-Mouse IgG H&L (Alexa Fluor® 568) (Abcam, #ab175473) was injected into the µ-Slide 8 well (Ibidi, #80826) and kept at a 90°-degree angle for 90 minutes at RT. Next, 150 µL of gel containing 10,000 HSJD-DIPG-07 cells was injected above the solidified layer of empty gel in the µ-Slide 8 well (Ibidi, #80826) and kept at a 90°-degree angle for 90 minutes at RT. 100 µL TSM containing 1 µg/mL Hoechst 33342 solution (ThermoFisher Scientific, #62249) was added to the chambers and the slide was incubated for 4 days at 37°C and 5% CO_2. The invasion of cells was monitored using the Leica Dmi8 S Platform Live cell microscope (Leica Microsystems, Wetzlar, Germany) on day 0 and day 4.

Angiogenesis slide hypothesis

The invasion assay was also performed in a µ-Slide angiogenesis (Ibidi, #81506) slide, where it was hypothesised that the structure of the slide would facilitate the establishment of evenly distributed layer of cells for imaging purposes. The µ-Slide angiogenesis (Ibidi, #81506) slide contained three horizontal layers of HyStem®-HP (Advanced Biomatrix, #GS315) matrix: a layer with 3 µL of BacMam 2.0 (ThermoFisher Scientific, #C10509), a buffer layer, and a layer with 10,000 HSJD-DIPG-07 cells. 10 µL of gel containing 10,000 HSJD-DIPG-07 cells was pipetted into the µ-Slide angiogenesis (Ibidi, #81506) slide and left to solidify for 90 minutes at RT. Next, 10 µL of empty gel was pipetted above the solidified layer of gel in the µ-Slide angiogenesis (Ibidi, #81506) slide and left to solidify for 90 minutes at RT. The final 10 µL layer of gel containing BacMam 2.0 (ThermoFisher Scientific, #C10509) was pipetted above the solidified layers of gel in the µ-Slide angiogenesis (Ibidi, #81506) slide and left to solidify for 90 minutes at RT. 40 µL TSM containing 1 µg/mL Hoechst 33342 solution (ThermoFisher Scientific, #62249) was added to the angiogenesis slide which was incubated for 4 days at 37°C and 5% CO_2. The invasion of cells was monitored using the Leica Dmi8 S Platform Live cell microscope (Leica Microsystems, Wetzlar, Germany) on day 0 and day 4.

Gel slice hypothesis

It was hypothesised that the layer system hindered the discernment between migrating and non-migrating cells because of the limitations associated with establishing level layer of matrix. Therefore, 300 µL of HyStem®-HP (Advanced Biomatrix, #GS315) matrix containing 3 µL

BacMam 2.0 (ThermoFisher Scientific, #C10509) was pipetted into a 24-well plate (Sarstedt, Numbrecht, Germany, #83.3922) and left to solidify for 90 minutes at RT. A surgical scalpel (Swann-Morton, Sheffield, England, # 6601) was used to create two perpendicular slices in the gel in the shape of a cross. 5 µL TSM containing 100,000 cells was carefully pipetted into the slices made into the gel. 500 µL TSM was added on top of the gel which was incubated for 4 days at 37°C and 5% CO_2. The invasion of cells was monitored using the Leica Dmi8 S Platform Live cell microscope (Leica Microsystems, Wetzlar, Germany) on day 0 and day 4.

PDMS mould invasion assay

In collaboration Professor Monique den Boer and her team, a polydimethylsiloxane (PDMS) sheet (Amazon) was used to create a mould in which the invasion assay could be performed in. A 6mm biopsy puncher (Merkala, #62506) was used to make two circular holes connected by a 1 mm x 1 mm bridge, which was created using a scalpel. The punctured PDMS mould was then sculptured into a circular format so that the entirety of the mould fit on a single 22 mm circular glass coverslip (Electron Microscope Sciences, #72224-01). Pressure was applied on the mould and cover slip before placing the coverslips onto a hot plate for 2 hours at 80°C. The moulds were rinsed with DI water before being stored in a petri dish until needed. On the day of cell seeding, the moulds were placed under UV for at least 20 minutes. Following this, the Matrigel Matrix (Corning, #354248)/ HyStem®-HP (Advanced Biomatrix, #GS315) gel was prepared, and different quantities of IUE murine cells were added into the gel and mixed using a pipette tip as a stick (this step is necessary to limit the formation of bubbles in the gel). Before the pipetting of cells into the moulds, a 1 mm x 1 mm piece of PDMS was carefully inserted into the bridge of the moulds to create a physical barrier, and the moulds were placed into separate 6-well well plates. Approximately 80 µL of gel containing cells was loaded into one side of the mould. The 6-well plates containing the moulds were incubated at 37°C and 5% CO_2 for 5 minutes to allow for partial solidification of the gel. Immediately after, the PDMS physical barrier was carefully removed and approximately 80 µL of empty gel was loaded into the remaining side of the mould. A 26G needle (Merkala) was then used to draw a bridge between the two gels and remove any air bubbles formed during the gel loading process. The moulds containing the gels were then incubated at 37°C and 5% CO_2 for 1 hour. 5 mL of TSM was added and the assay was left to incubate at 37°C and 5% CO_2 for 4 days. The plates were imaged using the Leica THUNDER Imager (Leica Microsystems) on day 0, day 4, day 8 and day 12. The images were processed using the Leica LAS X Life Science software and ImageJ.

Appendix 2: A table summarising the hypothesised methods for the high-throughput invasion assay including strengths and limitations

Method	Description	Strengths	Limitations
Three-layered 96-well plate	Three vertical layers of gel matrix: (1) Empty gel (2) Gel + BacMam 2.0 (3) Gel + cells	Vertical layers make distinction of migrating cells easier. BacMam 2.0 technology means that FACS could be used to isolate migrated cells.	Making three layers in small area was difficult. The layers were uneven making imaging difficult. BacMam 2.0 did not work.
8-well chambered slide	Two vertical layers of gel in a square shaped chamber: (1) Gel + BacMam 2.0 (2) Gel + cells	Vertical layers make distinction of migrating cells easier. Shape of chambers create even distribution of gel layers. BacMam 2.0 technology means that FACS could be used to isolate migrated cells.	Making vertical layers was difficult. The layers were uneven making imagining problematic. BacMam 2.0 did not work.
Angiogenesis slide	Cells seeded at the bottom of the chamber and two thin layers of gel matrix are seeded above: (1) empty gel (2) gel + BacMam 2.0	Thin layers means that cells must only migrate very short distances to encounter the BacMam 2.0. BacMam 2.0 technology can be used to isolate migrated cells using FACS.	BacMam 2.0 did not work. Horizontal layers made visualisation of migrated cells difficult.
Cross method	Scalpel used to create two perpendicular slices in the gel matrix containing BacMam 2.0 (in the shape of a cross)	Does not involve layers. BacMam 2.0 technology can be used to isolate migrated cells using FACS.	BacMam 2.0 did not work. When cell population becomes too dense it is difficult to distinguish the migrating cells.
PDMS mould	PDMS mould used to create two circles connected by a bridge. The cells are seeded into one circle, whilst the other circle remains empty.	Does not involve layers of BacMam 2.0. Cells that invade into the other circle can be isolated by punching out gel in invaded in circle and harvesting cells.	Large circle area often means cells 'retreat' from the bridge to establish dense networks before attempting to invade into the other circle. Starts to become hypoxic after 1 week.
Glass slide drop method	Two drops of gel are made on a glass slide. The drops are connected by a	Very easy to set-up and execute. Cells are seeded into a smaller area. Cells that enter the circles can be isolated by punching	Sometimes the cells crawl over the surface of the gel instead of invading the gel.

	bridge of gel containing cells.	out the circles and harvesting the cells.	

Appendix 3: Plasmid maps of constructs used in the project

<table>
<tr>
<td> 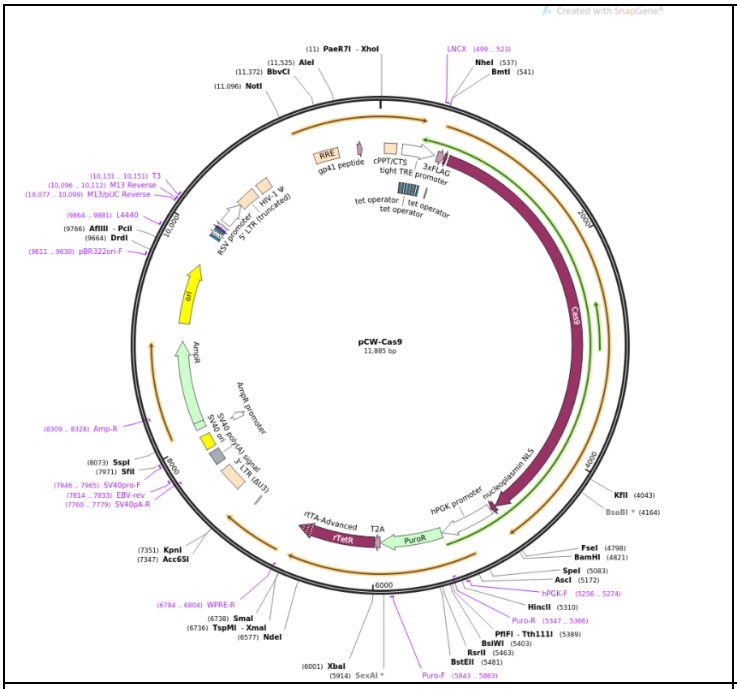
</td>
<td> 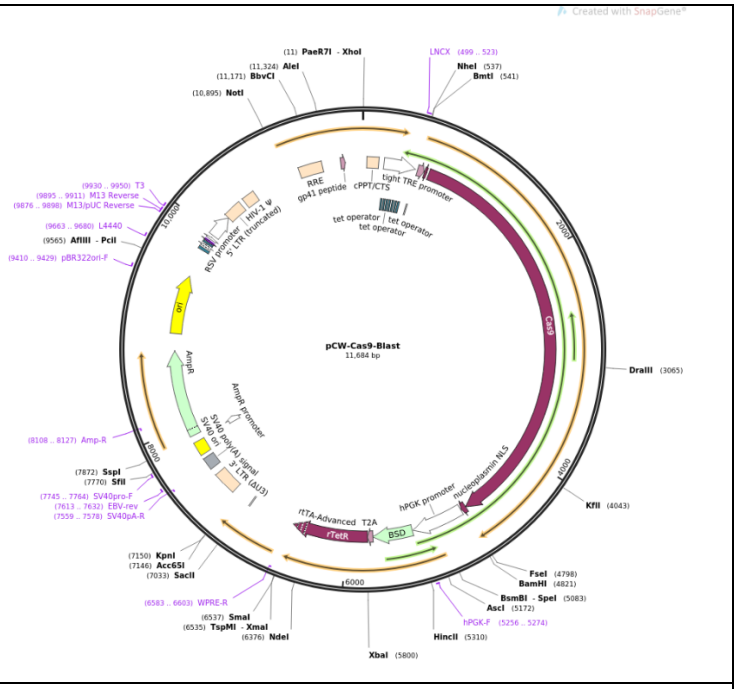
</td>
</tr>
<tr>
<td>pCW-Cas9 Puromycin (Addgene #50661)</td>
<td>pCW-Cas9 Blasticidin (Addgene #83481)</td>
</tr>
<tr>
<td> 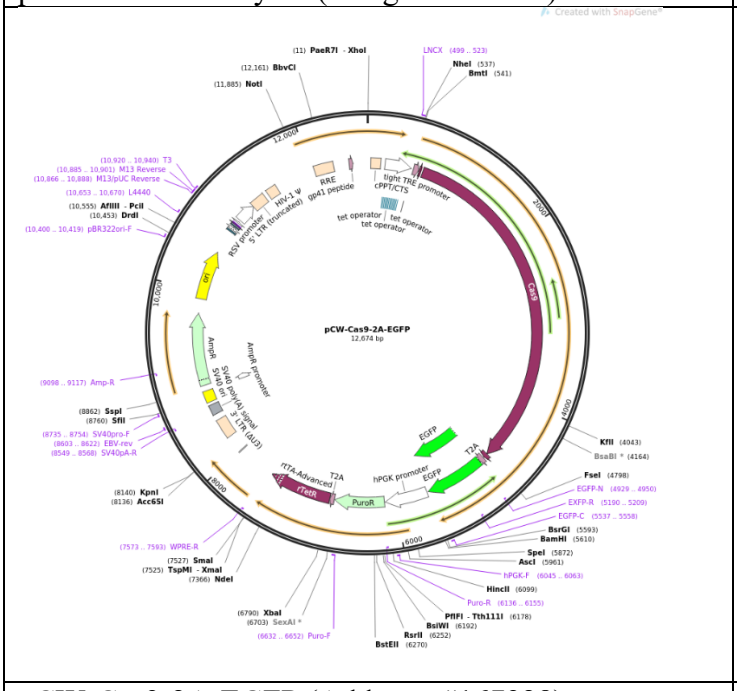
</td>
<td> 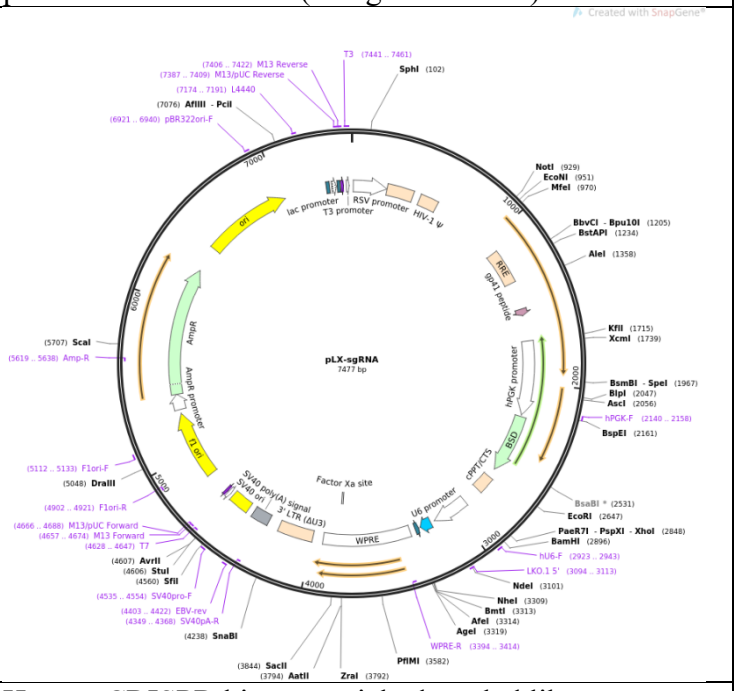
</td>
</tr>
<tr>
<td>pCW-Cas9-2A-EGFP (Addgene #167928)</td>
<td>Human CRISPR kinase-enriched pooled library (Addegene #51044) & Human CRISPR nucleosome-enriched pooled library (Addgene #51047)</td>
</tr>
</table>

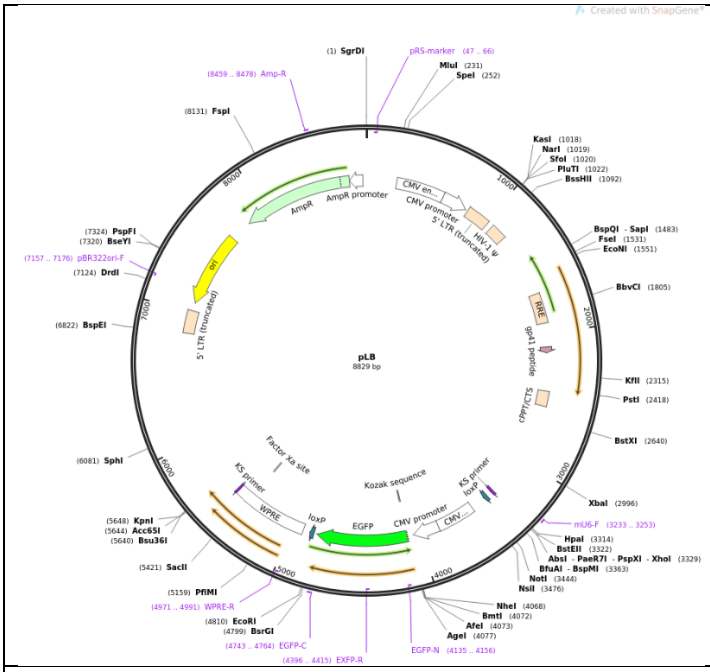	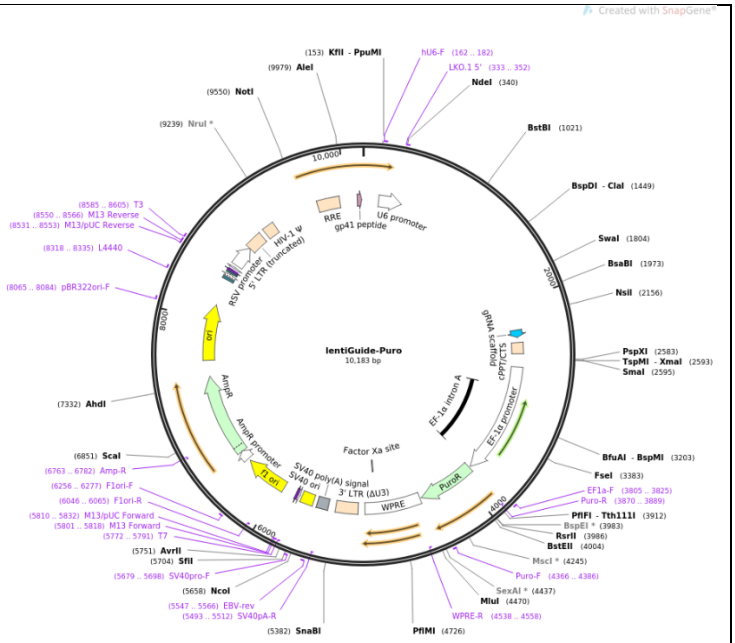
Human lentiviral CRISPR library v1 (Addgene #69763)	Mouse kinome CRISPR pooled library (Brie) (Addgene #75316)
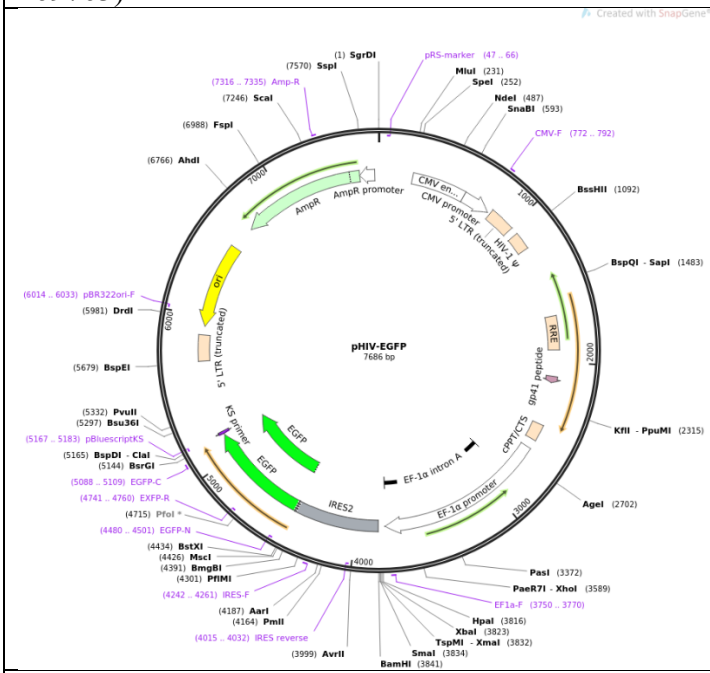	
pHIV-EGFP (Addgene #21373)	